UNIVERSITY OF CALIFORNIA, SAN DIEGO

Frequency and Phase Estimation for Application in Non–Optical Position Tracking of Maglev Vehicles

A Thesis submitted in partial satisfaction of the
requirements for the degree Master of Science

in

Engineering Sciences (Mechanical Engineering)

by

Alicia Powers

Committee in charge:

Professor Miroslav Krstić, Chair
Professor Robert R. Bitmead
Professor Mauricio de Oliveira

2009

The Thesis of Alicia Powers is approved, and it is acceptable in quality and form for publication on microfilm and electronically:

_____

_____

_____
Chair

University of California, San Diego

2009

To God,
for blessing me with wisdom beyond my years
To my parents,
for their time and devotion to my education
and for their encouragement and support of my efforts.

TABLE OF CONTENTS

LIST OF FIGURES

ACKNOWLEDGEMENTS

I would like to thank Professor Miroslav Krstić for his guidance in helping me complete this research and ensuring that I produced my highest quality work. General Atomics for allowing me to work on their Maglev system and Bogdan Borowy for his guidance of this project. Nima Ghods for all the time he spent helping me work through proofs and derivations and letting me interrupt his work to answer my questions. James Gray for helping me with the parameter estimation theory and showing me the proper formating of this thesis. All the guys in the office who made my time as a graduate student here at UCSD so enjoyable. Professor Bitmead and Professor de Oliveira for being on my defense committee.

VITA

2008	Bachelor of Science in Mechanical Engineering, University of California, San Diego
2009	Master of Science in Engineering Sciences (Mechanical Engineering), University of California, San Diego

ABSTRACT OF THE THESIS

Frequency and Phase Estimation for Application in Non–Optical Position Tracking of Maglev Vehicles

by

Alicia Powers

Master of Science in Engineering Sciences (Mechanical Engineering)

University of California San Diego, 2009

Professor Miroslav Krstić, Chair

This thesis considers how the position of a magnetic levitation train can be found non-optically using signal processing techniques. An overview of magnetic levitation trains is given, including an explanation of the necessity for non-optical position sensing. A least-squares with forgetting factor algorithm is derived, showing its convergence and stability. The input signal is manipulated so that the least-squares algorithm can be applied. Extremum seeking is introduced and utilized for phase estimation of the high frequency signal. When adding noise to the incoming signal, the frequency estimates remain accurate if the forgetting factor is allowed to vary proportional to the slope of the estimate. Additive noise has little effect on the extremum seeking phase estimate. The frequency and phase estimation is combined to reconstruct an estimate of the carrier signal to demodulate the signal and extract the position of the train.

1

Introduction

Magnetic levitation (maglev) trains as an advancing technology for providing a new means of transportation have steadily gaining interest in the United States over the past several years. Although maglev trains, first conceived of in the mid–sixties, have been in testing and operation for the past two decades, there still remain many areas for improvement. There is still debate and discussion on what technologies should be utilized in the three main areas necessary for maglev operation: levitation support, propulsion, and guidance.

Linear Synchronous Motors (LSMs) are one of the more common methods for providing the propulsion component to the maglev system. The ability to accurately track the train's position as it moves along the track provides essential information for the LSM controller. If the position information is inaccurate, the LSM will not synchronize properly, putting the magnetic field out of alignment with the applied current, which results in zero thrust. The various methods proposed to track the train's position include: optical encoders, magnetic encoders, and signal processing. The component chosen to determine the train's horizontal position must be accurate for signals with variation in amplitude and large levels of noise, in addition to having a knowledge of absolute position. General Atomics currently uses an optical sensor to follow the train's position. The optical encoder flags crossings between black and white stripes alongside the track as seen in figure 1.1 from [14]. The width of the black and white stripes is constant and has a length corresponding to a known horizontal displacement of the train. One difficulty with using an optical encoder is the likelihood of failure should dust, dirt, snow, or any substance interfere with the encoder's ability to distinguish between the stripes. In this case the encoder will not count properly and the position of the train will be inaccurate. In addition, the

Figure 1.1: Optical Encoder Method of Position Tracking

optical encoder does not give absolute position but requires synchronization. Although a magnetic encoder does not have a problem of inaccuracy due to substances on the track, the presence of large magnetic fields for lift could cause difficulty in detecting the correct magnetic flux and the issue of absolute position is not resolved. Hence, a more robust method is needed to track the train's position. Currently, MagneMotion uses LSMs for many types of applications, including maglev trains but also for elevators and conveyors. Their position tracking of the moving component is determined through non-optical means. Using signal processing methods, the three coil windings, which create the basis for the LSM, can also be used for position tracking. The coils operate at the same frequency but with phase offsets of 120° between each, plus an addition phase offset corresponding to the position of the train. The pattern of three coils with phase offsets is repeated over the length of the track. By transmitting a high frequency, ten kilohertz range, carrier signal from the train to the LSM coils on the track, the low frequency sinusoid of the coils receives the high frequency carrier, creating a modulated signal. This modulated signal can be used to find the position of the train, by demodulating the signal so that only the low frequency LSM signal remains. Non-optically detecting the position has several benefits: effectively operating in various weather conditions, high signal to noise ratio, absolute position measurements, and low power levels required to generate the carrier signal. The objective of this thesis is to develop a robust

method for estimating the position of the train using more novel signal processing techniques. This work will help to further the transfer of General Atomics' position estimation from optical to non-optical.

1.1 How Magnetic Levitation Trains Work

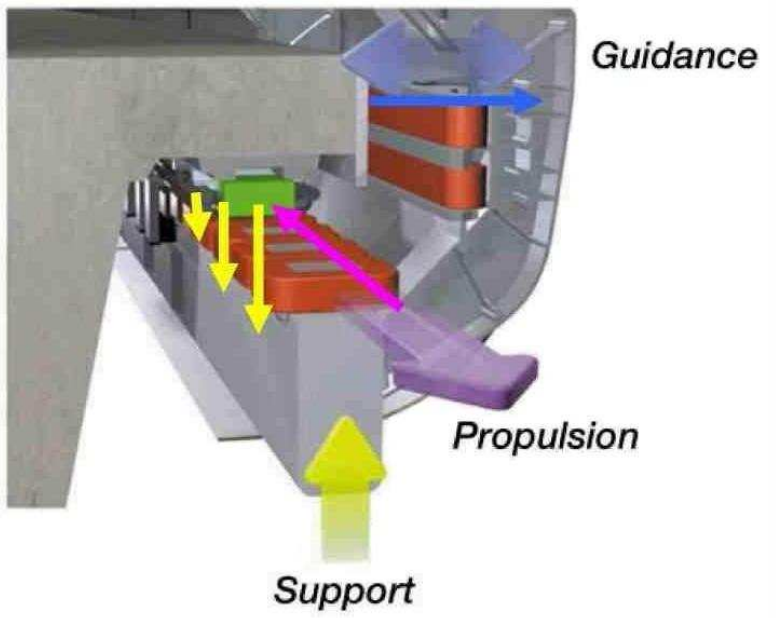

Figure 1.2: The Three Components of a Maglev System from [17]

Maglev trains operate using three main components: levitation support, guidance, and propulsion, as shown in figure 1.2 from [17]. There are many ways to design these components depending on the speed of the train, building costs, operating costs, and many other factors. The operating speed of a train is broken into two categories, high-speed intercity and urban. Germany's Transrapid operating in Shanghai China and Japan's HSST and JR–maglev are the most well known high speed trains. Japan Railways Group holds the highest speed reached by a train, operating at 581km/hr (361mi/hr). Several projects in the United States are currently investigating lower speed urban trains but none are currently used for commercial or public transport.

1.1.1 Levitation

The main methods used for levitation include: Electro-Magnetic Suspension (EMS), Electro-Dynamic Suspension (EDS), and Stabilized Permanent Magnet Suspension (SPM). The EMS uses electromagnets on the train to repel away from the track, which is made of iron or some other magnetic material. The gap size between the train and track is around 15 millimeters. This requires a highly tuned control system to monitor and adjust the electrical current sent to the electromagnets on the train so that the gap between the train and the track remains constant. The necessity of maintaining this minimal gap is an area of concern since the system is inherently unstable and vibrations from the train or track add variation to the gap size, which causes greater difficulties for the controller. A positive benefit to using EMS is the minimal magnetic field that surrounds the train, limiting the magnetic exposure of the passengers. In addition, EMS has proved reliable and can maintain stability at high speeds while requiring no additional landing wheels at low speeds. The EDS method uses repelling magnetic forces between the train and track, which are created through various combinations of permanent magnets and electromagnetic coils. The magnetic flux created between the track and the train is not strong enough at zero speed to lift the train, thus secondary landing gear is needed when the train stops at stations. Once the train reaches a certain speed, the magnets can lift the train off the track. The benefit of the EDS is the large air gap between the train and track which remains stable and allows for large load capacity. The use of high temperature superconducting magnets on the train, cooled by liquid nitrogen, makes it possible to levitate the train without the need for a large electrical power supply on the train itself. The main drawback of EDS is the large magnetic field that bleeds into the passenger cabin, requiring magnetic shielding inside the train, otherwise all magnetic devices (computers, credit cards) will become demagnetized. SPM uses permanent magnets arranged in a Halbach array for both the train and track. Therefore, no electricity is required for levitation, making the train more cost efficient and minimizing electromagnetic drag. Although it still requires wheels to support the train at zero speed, it is able to maintain levitation at slow speeds, increasing the amount of levitation time over the EDS design. The main benefit of using SPM is that the magnetic field does not extend beyond the region between the train and track, resulting in no magnetic exposure of the passengers. Also, there is no energy consumption used in the levitation component of the train, reducing the

operating cost substantially.

1.1.2 Guidance

The electromagnets used to create levitation in EMS and EDS systems also provide guidance since the electromagnets wish to be centered over the track's magnetic field. Therefore, no additional guidance is needed for these two designs. The SPM design requires additional guidance to keep the train centered over the track. Electromagnetic coils placed on the bottom of the permanent magnets on the train provide guidance through sending a small amount of current through the coils. This current only needs to be sent when the train is drifting away from the center of the track or going around a curve and since the coils do not have to produce any upward lift force, the energy consumption is very small.

The guideway incurs a large portion of the building costs for maglev systems, since many of the electronics and controls are housed in the guideway. The guideway must be designed to withstand vibrations from the train as it moves along the track and ensure minimal deflection, since any large deflections in the guideway cause additional noise in the sensor readings. In addition, the guideway must require minimal maintenance and have a life time of 80 – 100 years [17].

1.1.3 Propulsion

The two main propulsion techniques, Linear Induction Motors (LIMs) and Linear Synchronous Motors (LSMs), are both used in the currently operating trains. Japan HSST uses a LIM for propulsion while Germany's transrapid uses a LSM. In EDS trains, the magnets on the train and electromagnets on the track can provide both lift and thrust, using a LSM. For EMS and SPM trains, thrust is not correlated with lift, thus additional methods using LIM, LSM, or non–magnetic propulsion must be added. A LIM takes a conventional linear inductor machine and unrolls it to create horizontal displacement rather than angular displacement. In a single sided topology, in order to have continuous action, the stator and the secondary must be different lengths and most applications choose the linear stator to be short and the linear secondary to be long. This is best incorporated into the EMS design, since the coils on the train create a magnetic field, which induces a current in the passive metal plates on the track. The advantages of using a single sided linear induction motor is

the ability to provide greater thrust independent of friction, smaller turn radius, and propulsion up steep slopes [21]. One disadvantage of LIMs is the increased weight of the train, putting a limit on the maximum achievable speed and reducing the overall operating efficiency. Since the secondary component is passive, the amount of power required to create propulsion is much larger than for LSMs and the gap between the stator and the secondary must be small [11]. In addition, the reactor plate which receives the current can become overheated reducing its structural integrity. An alternate method uses a double sided topology with the stator extending the length of the track and the secondary attached to the carriage as a simple plate [5]. The benefit of this method is the passivity of the train, requiring no high voltage components on board the train. A concern with this design is the increased constraint on the veritcal movement of the train, since the train has to stay within the small slot between the two stator plates. The alternative magnetic propulsion option, LSM, has higher building cost but greater overall efficiency and less long term costs. The LSM uses electromagnetic forces through electrical coil windings on the track to propel the train. Since the moving magnetic field is located on the track, the onboard power is reduced and the vehicle is lighter. In addition, because the coil windings do not have to induce a current in the secondary component the amount of power consumption required is less than for LIMs [11]. A *variable reluctance* LSM uses the difference in the reluctance of the d and q-axis and the moving magnetic field to generate propulsion. The speed of the train is proportional to the synchronous speed of the current flow through the coils, controlled by varying a low frequency sinusoid or Pulse Width Modulator (PWM). The necessity of knowing the position of the train is the main drawback to using LSMs. Position feedback information is used to precisely synchronize the coil current with the moving magnetic field on the train [6]. Without proper synchronization with the traveling magnetic field, no propulsion occurs; therefore, knowing the position of the vehicle is essential.

1.2 Current Signal Processing Techniques

For this application, the input signal contains two modulated sinusoids; one of which is a high frequency signal from the train and the other a low frequency signal from the coils, which contains the position of the train as the phase offset. Using demodulation, the undesired carrier signal is removed and the sinusoid containing

the position information is isolated. However, the frequency and phase of the carrier signal must be known before the signal can be demodulated. Since initially only the order of magnitude for the frequency is known, both frequency and phase must be estimated more accurately. The use of demodulation to separate two sinusoids is a commonly used technique in communication systems. In a typical radio application, the transmitted signal frequency is known and the phase of the signal must be estimated in order to accurately demodulate the signal. Phase locked loops are one of the more common methods for finding the phase and are widely used in all types of communication applications [1]. [13] compares the robustness, convergence rate, and accuracy of various controllers in the phase locked loop. Adaptive filters used for phase estimation is examined in [10]. In this thesis an alternate method for phase identification will be examined using the nonlinear property of the sinusoidal signal.

Frequency estimation is commonly used for sonar application. For post processing the data, [15] uses periodograms as a basis for finding the frequency of sinusoids close to zero or two sinusoid close to each other in frequency. In other types of application such as vibration control, disk drives, and magnetic bearings [9], the frequency of a signal needs to be identified in real time. The various techniques for online estimation of frequencies include notch filters [16], frequency locked loops, adaptive filters, and Extended Kalman Filters [18]. The work done by [2, 8, 12, 20], identifies the frequency of single sinusoidal and additive sinusoidal signals using observers. In this research, frequency estimation will be extended to the multiplicative sinusoid case using a least-squares technique.

1.3 Contributions and Contents of Thesis

Demodulation is a well known and highly established method, which can be utilized to separate the two sinusoids and will in this application lead to position tracking of the train. Prior to demodulation, the frequency and phase of the undesired sinusoid must be estimated given limited knowledge of the frequency and no knowledge of the phase. This thesis provides an overview on how to estimate the frequency and phase of modulated sinusoids, $\cos(\omega_1 t + \phi_1) \cdot \cos(\omega_2 t + \phi_2)$.

First, the signal processing method used to create the modulated signal is described. An overview of the current non-optical method for locating the train is

examined to provide an understanding of which variables are desired and how the signal can be manipulated. Then the new method examined in this thesis will be introduced.

The initial step in the demodulation process is estimating the frequency, which will be done through parameter estimation. First the derivation for parameter estimation is examined, using a least squares cost function. An exponential multiplier is introduced into the least-squares cost function, denoted as the forgetting factor, to focus the cost function on the most recent data, thereby increasing the convergence rate from polynomial to exponential. The proof of stability and convergence is reviewed, using the persistence of excitation condition. A comparison between the *continuous-time recursive least–squares algorithm with forgetting factor* and the continuous time Kalman filter will be examined and concluded that the least–squares algorithm is superior for this application.

In order to utilize the least squares algorithm to estimate the frequencies of the modulated sinusoids, the frequencies must be put in a parametric relationship with the input. Applying a trigonometric identity transforms the multiplicative sinusoids into an additive sinusoidal relationship and using the derivatives of the sinusoids, the least–squares algorithm is applied. Simulation results confirm the stability and convergence of the parameters. In order to handle the addition of noise to the signal, the forgetting factor is changed from a constant to a variable that is adjusted online. This allows for quick convergence and reduces the noise effects of the zero gradient regions.

The phase estimation is done using extremum seeking. Using the local maximum of cosine at zero degrees, the error between the actual and estimated phase of the high frequency signal is minimized. A proof of extremum seeking will be examined to ensure stability of the phase estimate. Simulation results confirm the stability both without noise and in the presence of additive noise.

2

Theory of Signal Processing

The Linear Synchronous Machine with vector control produces the thrust component of the maglev system and operates similarly to a DC motor. A magnetic field propagates from the magnetic Halbach array on the chassis of the train. By applying a current in the coil windings on the track, a second moving magnetic field is generated. Since opposite poles attract, the magnetic field on the train is drawn toward the opposite magnetic field created by the coils. Hence the train is pulled along as the coils continue to move the magnetic field down the track. As shown in figure 2.1, the current from the coils creates a magnetic field and the magnetic field from the train is drawn down the track, which propels the train forward. As long

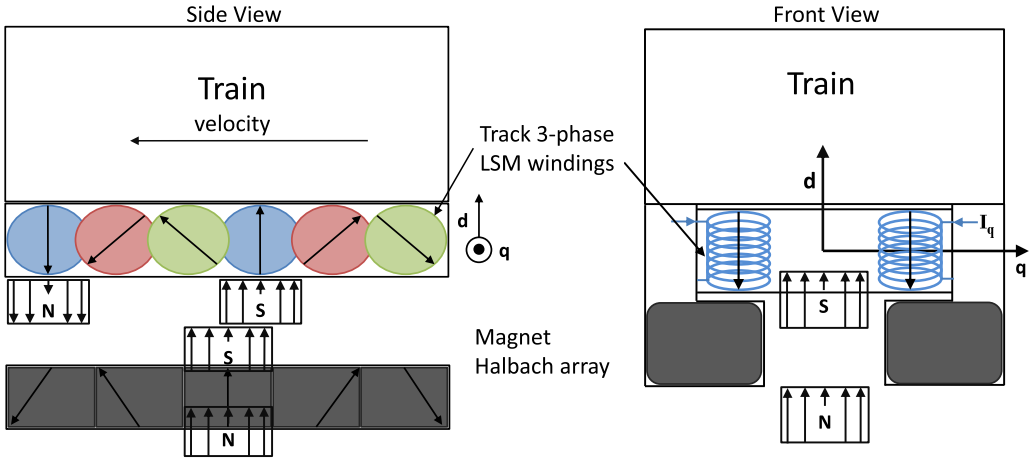

Figure 2.1: Diagram of Magnetic Flux and Current in the d and q axis, Creating Propulsion

the magnetic field from the train remains perpendicular to the q-axis, the current applied in the q-axis direction produces optimal thrust efficiency. Knowing the po-

sition of the train allows synchronization of the current sent to the coils and propels the train forward.

In order to detect the position of the train, signal processing methods are utilized. A coil drive mounted on the vehicle transmits a high frequency signal, denoted as the carrier signal, to the three-phase windings of the LSM. The resonant circuitry mounted across the windings is tuned to the frequency of the signal sent from the train. Figure 2.2 shows the basic concept of the signal transmission from the train to the coils. The term three-phase windings of the coils denotes the three alternating phase shifts of the coils' sinusoidal signal. These offsets in phase create an orthogonal basis for the position signal. The magnetic flux created by the high frequency signal penetrates the LSM windings and the resulting voltage from each of the three-phase coils is proportional to a modulated signal, in phase with the respective coil sinusoid.

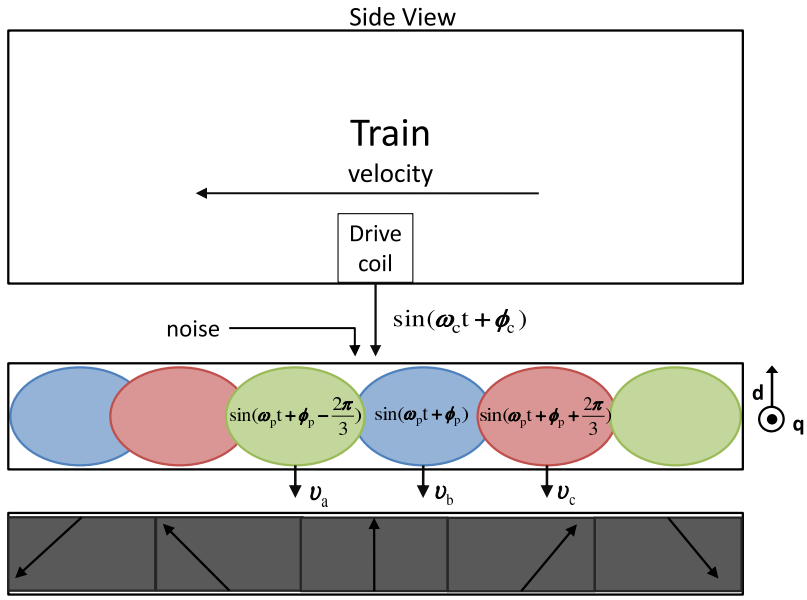

Figure 2.2: Signal Transmission from Train Drive Coil to Three-Phase LSM Windings

2.1 Current Non-Optical Position Detection

The following analysis reviews the method for position detection currently under testing, as laid out by [3]. The train moves at a speed v which relates to an angular frequency of $\omega_p = 2\pi\frac{v}{\lambda}t$. The high frequency signal produced by the drive coil on

the train creates a magnetic flux proportional to a voltage,

$$v_c \propto \sin(\omega_c t + \phi_c).$$

The three-phase windings on the track have a density with sinusoidal distribution, at a frequency corresponding to the train's velocity. The phase offsets of the three coils are located at, 0, $-\frac{2\pi}{3}$, and $\frac{2\pi}{3}$ radians in order to be equally spaced over the 2π radians of a circle. An additional phase shift present in the sinusoid, ϕ_p, corresponds to the horizontal position of the train,

$$n_x \propto \sin(\omega_p t + \phi_p + \phi_x), \quad x = a, b, c \quad \phi_x = \begin{cases} -\frac{2\pi}{3} & x = a \\ 0 & x = b \\ \frac{2\pi}{3} & x = c \end{cases}. \tag{2.1}$$

When the signal from the train is received by the coils on the track, the resulting voltage at the coils is proportional to a modulated sinusoid between the carrier signal and winding densities,

$$v_x \propto \sin(\omega_c t + \phi_c)\sin(\omega_p t + \phi_p + \phi_x), \quad x = a, b, c \quad \phi_x = \begin{cases} -\frac{2\pi}{3} & x = a \\ 0 & x = b \\ \frac{2\pi}{3} & x = c \end{cases}. \tag{2.2}$$

The amplitude of the signal is not constant as the distance between the transmitter and coils changes due to vibrations. This variation in amplitude must be included in the modulated signal. Common mode noise is also present in the transmission, thus a more realistic equation for the modulated signal becomes,

$$v_x \propto A(t)\sin(\omega_c t + \phi_c)\sin(\omega_p t + \phi_p + \phi_x) + N_{cm}, \quad x = a, b, c. \tag{2.3}$$

The three windings on the track create the orthogonal basis of the modulated signal, which allows for the common mode noise to be removed. Removing the common mode noise and using a trigonometric identity, equation (2.3) is rewritten,

$$v_x \propto A(t)[\cos((\omega_c - \omega_p)t + \phi_c - \phi_p - \phi_x) - \cos((\omega_c + \omega_p)t + \phi_c + \phi_p + \phi_x)]$$

In order to make the vector control uncorrelated between the d and q axis, the voltages must be transformed from a, b, c to the d-q frame. A receiver signal with arbitrary phase multiplied with the voltages of the three coils transforms the signals

into the d-q frame.

$$
\begin{aligned}
v_d \propto & \sum_{x=a,b,c} A(t)\sin(\omega_r t + \phi_r + \phi_x)\cdot \\
& [\cos((\omega_c - \omega_p)t + \phi_c - \phi_p - \phi_x) - \cos((\omega_c + \omega_p)t + \phi_c + \phi_p + \phi_x)] \\
v_q \propto & \sum_{x=a,b,c} A(t)\cos(\omega_r t + \phi_r + \phi_x)\cdot \\
& [\cos((\omega_c - \omega_p)t + \phi_c - \phi_p - \phi_x) - \cos((\omega_c + \omega_p)t + \phi_c + \phi_p + \phi_x)]. \qquad (2.4)
\end{aligned}
$$

Through expansion of (2.4) using trigonometric identities, the sinusoids with common modes from the phase offsets can be removed. The magnitude of the voltage in the d and q directions reduce to

$$
\begin{aligned}
v_d \propto & A(t)[\sin((\omega_c + \omega_r - \omega_p)t + \phi_c + \phi_r - \phi_p) \\
& + \sin((\omega_c - \omega_r + \omega_p)t + \phi_c - \phi_r + \phi_p)] \\
v_q \propto & A(t)[\cos((\omega_c + \omega_r - \omega_p)t + \phi_c + \phi_r - \phi_p) \\
& - \cos((\omega_c - \omega_r + \omega_p)t + \phi_c - \phi_r + \phi_p)]
\end{aligned}
$$

A low pass filter removes the high frequency signal to reduce the voltage equations even more, but the filter also adds a phase shift,

$$
\begin{aligned}
v_d &\propto A(t)\sin((\omega_c - \omega_r + \omega_p)t + \phi_c - \phi_r + \phi_p + \phi_{fF}) \\
v_q &\propto -A(t)\cos((\omega_c - \omega_r + \omega_p)t + \phi_c - \phi_r + \phi_p + \phi_{fF}) \qquad (2.5)
\end{aligned}
$$

Looking at (2.5), taking the ratio $\frac{-v_d}{v_q}$ allows the voltages in the d and q directions to be combined into a single tangent function. The forward angle is defined by removing the trigonometric function, retaining only the frequency and phase components,

$$
\phi_F = \arctan\left(\frac{-v_d}{v_q}\right) = (\omega_c - \omega_r)t + \omega_p t + \phi_c - \phi_r + \phi_p + \phi_{fF} \qquad (2.6)
$$

In addition to analyzing the forward angle by taking the positive component of the receiver frequency, the negative frequency values can also be evaluated. The same procedure starting from equation (2.4) is followed, except ω_r and ϕ_r are replaced by $-\omega_r$ and $-\phi_r$. As a result of the change in signs, the magnitude of the voltages in the d and q directions become,

$$
\begin{aligned}
v_d &\propto A(t)\sin((\omega_c - \omega_r - \omega_p)t + \phi_c - \phi_r - \phi_p - \phi_{fB}) \\
v_q &\propto A(t)\cos((\omega_c - \omega_r - \omega_p)t + \phi_c - \phi_r - \phi_p - \phi_{fB}).
\end{aligned}
$$

These two trigonometric functions can be combined to define the backward angle,

$$\phi_B = \arctan\left(\frac{-v_d}{v_q}\right) = -(\omega_c - \omega_r)t + \omega_p t - \phi_c + \phi_r + \phi_p + \phi_{fB}. \tag{2.7}$$

By adding (2.6) and (2.7) the frequency and phase of the carrier and receiver signals are eliminated. In addition, if the phase offsets from the filters are known, they can also be subtracted from the forward and backward angles, leaving only the frequency and phase corresponding to the train,

$$\phi_F + \phi_B - \phi_{fF} - \phi_{fB} = 2(\omega_p t + \phi_p) \tag{2.8}$$

2.2 Position Detection Using Demodulation

An alternative method to determining the position is to eliminate the high frequency signal from the modulated input. This is done through demodulation, which multiplies the input with the high frequency carrier signal and applies a low pass filter to output only the low frequency sinusoid. In order to demodulate the signal the frequency and phase of the carrier must be determined. Hence the objective of this research is to estimate the frequency and phase of the carrier signal, given the modulated input and the order of magnitude of the carrier frequency. Once the sinusoid from the coils is separated from the carrier, the phase can be extrapolated. The benefit of demodulation over the d-q transformation approach is the increase in signal to noise ratio. In addition, only one of the coil sinusoids is needed, rather than all three.

3

Parameter Estimation

In this chapter the *continuous-time recursive least–squares algorithm with forgetting factor* is derived. First, the system is placed in a parametric form. The cost function uses the parametric form to derive the equations forF updating the parameter estimates. The conditions of persistence of excitation are placed upon the system. Then the stability proof and convergence of the algorithm is reviewed. Lastly, the least-squares algorithm is compared to the continuous time Kalman filter.

3.1 Parametric Model Form

The parametric model of an input output system is given by

$$Y = \Phi^T \theta. \tag{3.1}$$

This is derived from a polynomial relationship between the input u and the output y,

$$b_0 + b_1 \frac{dy}{dt} + \cdots + \frac{d^n y}{dt^n} = a_0 + a_1 \frac{du}{dt} + \cdots + a_{n-1} \frac{d^{n-1} u}{dt^{n-1}}. \tag{3.2}$$

The parameters b and a are the values that need to be estimate with the output y as the only known value in the polynomial relationship. The unknown parameters, a_k, b_k, where $0 \leq k \leq n$, are grouped together on the right hand side, while any values independent of the parameters are moved to the left hand side. The unknown parameters are arranged in a column vector, θ, and the inputs/outputs which correspond to the unknown parameters are arranged in a second vector, Φ.

$$\theta = [a_0, a_1, \cdots, a_{n-1}, b_0, \cdots, b_{n-1}]^T \tag{3.3}$$

$$\phi = \left[u, \frac{du}{dt}, \cdots, \frac{d^{n-1}u}{dt^{n-1}}, -y, \cdots, -\frac{d^{n-1}y}{dt^{n-1}}\right]^T. \tag{3.4}$$

The known portion of the equation on the left hand side, $\frac{d^n y}{dt^n}$, is independent of any parameters and therefore equation (3.2) is rewritten as,

$$\frac{d^n y}{dt^n} = \phi^T \theta. \tag{3.5}$$

In general, one does not have information about the n$^{\text{th}}$ derivative of y, only y itself and having to take derivatives of a function is undesirable. By transforming the system into the Laplace domain, the need to know the derivative of y is removed by multiplying an n$^{\text{th}}$ order filter $\Lambda = s^n + \lambda_{n-1}s^{n-1} + \cdots + \lambda_0$ to both sides of (3.5). Equation (3.5) in the Laplace domain with the filter becomes

$$\frac{s^n}{\Lambda}[y] = \frac{1}{\Lambda}\phi^T \theta. \tag{3.6}$$

By defining $Y = \frac{s^n}{\Lambda}[y]$ and $\Phi = \frac{1}{\Lambda}\phi$, the parametric model of equation (3.1) is obtained.

3.2 Least Squares form of Adaptive Filter

Although there are multiple methods for parameter estimation, the least squares method was chosen for this application to allow for real time adjustment of the gain, including an exponential term to focus the gain on the most recent data. Although a pure least squares without the exponential term can be used, the convergence rate can be slow. Based on the least squares with forgetting factor approach found in [7] and Section 4.3.6 of [10], an overview of the derivation is reviewed.

The least–squares with forgetting factor algorithm uses the parametric form (3.1) to determine the error between the actual system and the estimated system, defining the estimated system as $\hat{Y} = \Phi^T \hat{\theta}$. The following cost function is minimized and used to update the parameter estimates,

$$J(\hat{\theta}) = \frac{1}{2}\int_0^t e^{-\beta(t-\tau)}[Y(\tau) - \Phi^T(\tau)\hat{\theta}(t)]^2 \, \mathrm{d}\tau + \frac{1}{2}e^{-\beta t}(\hat{\theta} - \hat{\theta}_0)^T Q_0 (\hat{\theta} - \hat{\theta}_0). \tag{3.7}$$

Defining $Q_0 = Q_0^T > 0$, $\beta > 0$ and $\hat{\theta}(0) = \hat{\theta}_0$, this is the generic form of the least squares with forgetting factor cost function. Note that β is exponentially related to the error, which causes the cost to focus only on the most recent data and

removes the weight of the previous errors exponentially. The additive term penalizes the initial error and is also exponentially decaying at the rate βt. By defining Y, $\Phi \in \mathcal{L}_\infty$, $J(\hat{\theta})$ becomes a convex function of $\hat{\theta}$ in $\mathcal{R}^n$ at each time t. Therefore the local minimization of $Y - \Phi^T\hat{\theta}$ is also a global minimum and consequently, $\nabla J(\hat{\theta}) = 0$. Setting the gradient of (3.7) to zero,

$$\nabla J(\hat{\theta}) = -\int_0^t e^{-\beta(t-\tau)}\Phi(\tau)[Y(\tau) - \Phi^T(\tau)\hat{\theta}(t)]\,\mathrm{d}\tau + e^{-\beta t}Q_0(\hat{\theta} - \hat{\theta}_0) = 0. \tag{3.8}$$

Solving (3.8) for $\hat{\theta}$ reveals the *nonrecursive least-squares* algorithm,

$$\hat{\theta} = \Gamma[e^{-\beta t}Q_0\hat{\theta}_0 + \int_0^t e^{-\beta(t-\tau)}\Phi(\tau)Y(\tau)\,\mathrm{d}\tau], \tag{3.9}$$

where

$$\Gamma = [e^{-\beta t}Q_0 + \int_0^t e^{-\beta(t-\tau)}\Phi(\tau)\Phi^T(\tau)\,\mathrm{d}\tau]^{-1} \tag{3.10}$$

and $Q_0 = Q_0^T > 0$ and $\Phi\Phi^T \geq 0$. Based on these conditions, $\Gamma(t)$ exists at each time t. Taking the inverse of the function is undesirable; thus, an alternate method for finding Γ is used. Starting with the identity,

$$\frac{d}{dt}(\Gamma\Gamma^{-1}) = \dot{\Gamma}\Gamma^{-1} + \Gamma\frac{d}{dt}\Gamma^{-1} = 0$$

and rearranging to derive the differential equation form,

$$\begin{aligned}\dot{\Gamma} = -\Gamma\frac{d}{dt}\Gamma^{-1}\Gamma &= -\Gamma(-\beta e^{-\beta t}Q_0 - \beta\int_0^t e^{-\beta(t-\tau)}\Phi(\tau)\Phi^T(\tau)\,\mathrm{d}\tau + \Phi\Phi^T)\Gamma \\ &= -\Gamma(-\beta\Gamma^{-1} + \Phi\Phi^T)\Gamma \\ \dot{\Gamma} &= \beta\Gamma - \Gamma\Phi\Phi^T\Gamma. \end{aligned} \tag{3.11}$$

Now Γ can be calculated by taking the integral of (3.11) and Γ^{-1} no longer needs to be calculated.

Putting $\hat{\theta}$ in a differential form creates a continuous time update algorithm. By taking the derivative of equation (3.9) with respect to time,

$$\begin{aligned}\dot{\hat{\theta}} &= \dot{\Gamma}\Gamma^{-1}\hat{\theta}(t) + \Gamma[-\beta(e^{-\beta t}Q_0\hat{\theta}_0 + \int_0^t e^{-\beta(t-\tau)}\Phi(\tau)Y(\tau)\,\mathrm{d}\tau) + \Phi Y] \\ &= [\beta\Gamma - \Gamma\Phi\Phi^T\Gamma]\Gamma^{-1}\hat{\theta}(t) + \Gamma(-\beta\Gamma^{-1}\hat{\theta}(t) + \Phi Y) \\ &= \beta\hat{\theta} - \Gamma\Phi\Phi^T\hat{\theta} - \beta\hat{\theta} + \Gamma\Phi Y \\ \dot{\hat{\theta}} &= \Gamma\Phi(Y - \Phi^T\hat{\theta}) \end{aligned} \tag{3.12}$$

Using equations (3.11) and (3.12), known as the *continuous-time recursive least–squares algorithm with forgetting factor*, the estimate $\hat{\theta}$ converges to θ and the gain is updated by Γ. Figure 3.1 shows the block diagram for the algorithm, with online tuning of Γ.

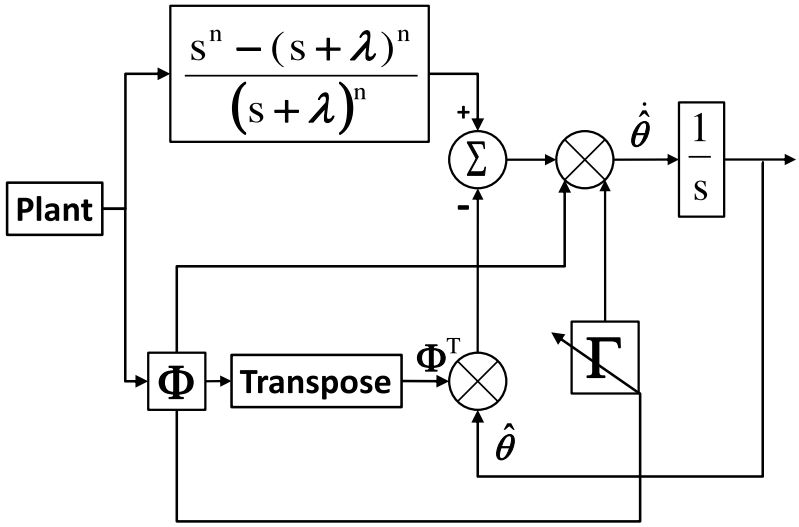

Figure 3.1: Block Diagram of Least–Squares Adaptive Filter

3.3 Stability Proof for Least–Squares

[7] goes into great detail about the proof of convergence and stability for the *continuous-time recursive least–squares algorithm with forgetting factor*. Since the pure least–squares with $\beta = 0$ is not used for this application, the proof of this algorithm will not be reviewed here. The least–squares with forgetting factor $\beta > 0$ will be summarized based on [7] and [10].

In order for $\hat{\theta}$ to converge to θ, Φ must satisfy the conditions of persistence of excitation and $\Phi(t) \in \mathcal{L}_\infty$. Persistence of Excitation is defined as:

Definition 3.1 ***Persistence of Excitation (PE):*** *A piecewise continuous signal vector $\Phi : \mathcal{R}^+ \to \mathcal{R}^n$ is PE in $\mathcal{R}^n$ with a level of excitation $\alpha_0 > 0$ if there exist constants $\alpha_1, T_0 > 0$ such that*

$$\alpha_1 I \geq \frac{1}{T_0}\int_t^{t+T_0} \Phi(\tau)\Phi^T(\tau)\,\mathrm{d}\tau \geq \alpha_0 I, \quad \forall t > 0. \tag{3.13}$$

The definition requires that $\Phi(t)$ vary over time so that the integral of $\Phi(\tau)\Phi^T(\tau)$ is uniformly positive definite over any time interval $[t, t + T_0]$.

Assuming that Φ satisfies the PE condition and knowing that

$$\frac{d}{dt}\Gamma^{-1} = -\Gamma^{-1}\dot{\Gamma}\Gamma^{-1},$$

the steady state value of Γ can be determined. Since $\dot{\Gamma}$ is known, $\frac{d}{dt}\Gamma^{-1}$ is written as

$$\frac{d}{dt}\Gamma^{-1} = -\beta\Gamma^{-1} + \Phi\Phi^T. \tag{3.14}$$

This ODE is solved,

$$\Gamma^{-1} = e^{-\beta t}\Gamma_0^{-1} + \int_0^t e^{-\beta(t-\tau)}\Phi\Phi^T \,\mathrm{d}\tau \tag{3.15}$$

and the integral on the right hand side is similar to that seen in the PE condition, equation (3.13). For $t > T$ and since $e^{-\beta t}\Gamma_0^{-1} \geq 0 \quad \forall t$, (3.15) is rewritten as an inequality,

$$\begin{aligned}
\Gamma^{-1} &\geq \int_0^t e^{-\beta(t-\tau)}\Phi\Phi^T \,\mathrm{d}\tau \\
&\geq \int_0^{t-T_0} e^{-\beta(t-\tau)}\Phi\Phi^T \,\mathrm{d}\tau + \int_{t-T_0}^t e^{-\beta(t-\tau)}\Phi\Phi^T \,\mathrm{d}\tau \\
&\geq e^{-\beta T_0}\alpha_0 T_0 I.
\end{aligned}$$

If $t < T_0$,

$$\begin{aligned}
\Gamma^{-1} &\geq e^{-\beta t}\Gamma_0^{-1} \geq e^{-\beta T_0}\Gamma_0^{-1} \\
&\geq \frac{1}{\lambda_{max}(\Gamma_0)} e^{-\beta T_0} I.
\end{aligned} \tag{3.16}$$

Defining

$$\gamma_1 = \min\left\{\alpha_0 T_0, \frac{1}{\lambda_{\max}(\Gamma_0)}\right\} e^{-\beta T_0}, \tag{3.17}$$

substitute (3.17) back into (3.16),

$$\Gamma(t)^{-1} \geq \gamma_1 I. \tag{3.18}$$

The upper bound for Γ^{-1} can be determined starting with (3.15) and using the upper bound of Φ from the PE condition.

$$\begin{aligned}
\Gamma^{-1} &\leq \Gamma_0^{-1} + \int_0^t e^{-\beta(t-\tau)}\Phi(t)\Phi^T(t) \,\mathrm{d}\tau \\
&\leq \Gamma_0^{-1} + \frac{1}{\beta}\alpha_1 T_0 I - \frac{1}{\beta}e^{-\beta t}\alpha_1 T_0 I \\
&\leq \Gamma_0^{-1} + \frac{1}{\beta}\alpha_1 T_0 I
\end{aligned}$$

Defining

$$\gamma_2 = \frac{1}{\lambda_{\min}(\Gamma_0)} + \frac{\alpha_1 T_0}{\beta}, \tag{3.19}$$

the upper bound for Γ^{-1} is defined as,

$$\Gamma(t)^{-1} \leq \gamma_2 I. \tag{3.20}$$

Now Γ^{-1} is bounded on both sides from equations (3.18) and (3.20),

$$\gamma_1 I \leq \Gamma(t)^{-1} \leq \gamma_2 I \tag{3.21}$$

and taking the inverse,

$$\gamma_2^{-1} I \leq \Gamma(t) \leq \gamma_1^{-1} I \tag{3.22}$$

Since Γ has both upper and lower bounds, it satisfies the condition $\Gamma \in \mathcal{L}_\infty$.

$\tilde{\theta}$ is defined as the error between the parameters and the estimates,

$$\tilde{\theta} = \theta - \hat{\theta} \tag{3.23}$$

and the derivative

$$\dot{\tilde{\theta}} = \dot{\hat{\theta}} \tag{3.24}$$

since the actual parameters are constant.

Now looking at the Lyapunov function

$$V = \tilde{\theta}\Gamma^{-1}\tilde{\theta}, \tag{3.25}$$

and taking the time derivative,

$$\begin{aligned}
\dot{V} &= \dot{\tilde{\theta}}^T\Gamma^{-1}\tilde{\theta} + \tilde{\theta}^T\dot{\Gamma}^{-1}\tilde{\theta} + \tilde{\theta}^T\Gamma^{-1}\dot{\tilde{\theta}} \\
&= 2\tilde{\theta}^T\Gamma^{-1}(-\Gamma\Phi\Phi^T\tilde{\theta}) + \tilde{\theta}^T(-\beta\Gamma^{-1} + \Phi\Phi^T)\tilde{\theta} \\
&= -\tilde{\theta}^T\Phi\Phi^T\tilde{\theta} - \beta\tilde{\theta}^T\Gamma^{-1}\tilde{\theta}.
\end{aligned}$$

Given that $\tilde{\theta}^T\Phi\Phi^T\tilde{\theta} \geq 0$, $\dot{V} \leq 0$ and the above equation can be reduced to the form,

$$\begin{aligned}
\dot{V} &\leq -\beta\tilde{\theta}\Gamma^{-1}\tilde{\theta} \\
&\leq -\beta V
\end{aligned} \tag{3.26}$$

or alternatively,

$$V(t) \leq V_0 e^{-\beta t}, \quad \forall t \geq 0. \tag{3.27}$$

Thus the exponential stability of the system is proved. To show that $\tilde{\theta}$ converges to zero, use (3.22) and (3.25) to bound $\tilde{\theta}$ by,

$$|\tilde{\theta}|^2\gamma_1 I \leq V \leq |\tilde{\theta}|^2\gamma_2 I. \tag{3.28}$$

Looking at the upper bound of $\tilde{\theta}$ and rearranging (3.28),

$$|\tilde{\theta}|^2 \leq \frac{1}{\gamma_1} V$$

and in addition, from (3.27) using the upper bound on V,

$$|\tilde{\theta}|^2 \leq \frac{1}{\gamma_1} V_0 e^{-\beta t}.$$

The upper bound for V_0 as shown in (3.28) gives the final inequality for $\tilde{\theta}$,

$$|\tilde{\theta}|^2 \leq \frac{\gamma_2}{\gamma_1} |\tilde{\theta}_0|^2 e^{-\beta t}. \tag{3.29}$$

Therefore $\lim_{t\to\infty} \tilde{\theta}(t) \to 0$ due to the negative exponential term, which means that $\hat{\theta} \to \theta$ exponentially.

3.4 Kalman Filtering

The Kalman Filter is well known for its stability and robustness and is widely applied in the areas of tracking and estimation. Given a state space representation of the input output relationship, the various vectors and matrices are easily inserted into the continuous Kalman Filter. The continuous time Kalman filter is laid out in section 8.2 of [19]. Starting with the state space representation,

$$\begin{aligned} \dot{x} &= Ax + Bu + w \\ y &= Cx + v, \end{aligned}$$

the Kalman filter estimates the values of x according to the following equations,

$$\begin{aligned} \hat{x}(0) &= E[x(0)] \\ P(0) &= E[(x(0) - \hat{x}(0))(x(0) - \hat{x}(0))^T] \\ K &= PC^T R_c^{-1} \\ \dot{\hat{x}} &= A\hat{x} + Bu + K(y - C\hat{x}) \\ \dot{P} &= -PC^T R_c^{-1} CP + AP + PA^T + Q_c, \end{aligned} \tag{3.30}$$

where R_c and Q_c are the variance of the Gaussian white noise signals w and v. When comparing (3.30) to that the least–squares algorithm (3.11) and (3.12), it is seen that if $\beta = 0$, the two have a compatible form by setting $A = 0$, $B = 0$, $Q_c = 0$,

$R_c^{-1} = \mathrm{I}$, $y = Y$, $x = \theta$, $P = \Gamma$, and $C^T = \Phi$. The Kalman filter can be rewritten using the variables of the least-squares algorithm as

$$\begin{aligned}
\hat{\theta}(0) &= E[\theta(0)] \\
\Gamma(0) &= E[(\theta(0) - \hat{\theta}(0))(\theta(0) - \hat{\theta}(0))^T] \\
K &= \Gamma\Phi \\
\dot{\hat{\theta}} &= K(Y - \Phi^T\hat{\theta}) \\
\dot{\Gamma} &= -\Gamma\Phi\Phi^T\Gamma.
\end{aligned} \tag{3.31}$$

It is interesting to note, that the differential equation for $\dot{x}$ from the input output equations is zero, which means that x is a constant. This is consistent with the derivation of the least–squares algorithm in which θ is the vector of parameters a_k and b_k which are defined as constants. Although the Kalman filter could be used instead of the adaptive filter, the lack of forgetting factor in the system causes a slower rate of convergence than using the least–squares with forgetting factor form of the adaptive filter. By analyzing the Kalman filter, the gain, K, is explicitly calculated and Γ is more apparent as representing the covariance matrix. In the Kalman filter, $\lim_{t\to\infty} \Gamma(t) = 0$ is necessary in order for the estimate to converge to the correct value since there is no forgetting factor present.

4

Parameter Estimation for Frequency

For estimating the frequency of a sinusoid, the main difficulty is that the desired parameter, frequency, is a function of the sinusoid rather than a multiplicative relationship. Based on the work done by [12, 8, 20, 2] through the use of derivatives, the frequencies are taken outside the sinusoids. However, in the above papers, the estimated frequencies are from additive sinusoidal inputs rather than the multiplicative input of this application. Thus, direct implementation of the current techniques cannot be used, but the basic theory of using the derivatives to put the parameters into a multiplicative relationship with the input signal can be applied. To put the multiplicative sinusoids into a parametric form, a trigonometric identity is applied to rearrange the signal into an additive sinusoidal form. Upon completion of this transformation, derivatives of the signal are used to take the frequencies outside the sinusoid and put them in a multiplicative relationship with the input signal. The signal is then placed in the parametric form and the least-squares algorithm is applied. Simulation results confirm the convergence and stability of the method.

4.1 Putting Modulated Signal in Additive Form

The input signal consists of two multiplicative sinusoids,

$$y = \cos(\omega_c t + \phi_c) \cdot \cos(\omega_p t + \phi_p). \tag{4.1}$$

For this application, the modulated signal is the result of the LSM coils receiver modulating with the high frequency signal sent from the coil drive on the train. ω_c

is defined as the frequency of the carrier signal and ω_p is the frequency of the LSM coil windings which corresponds to the velocity of the train. One can find both ω_c and ω_p according to the following procedure.

The input of (4.1) is in a multiplicative form; however, the signal is more easily manipulated if the sinusoids are additive. By applying a trigonometric identity, y can be rewritten in an additive sinusoidal form, although the frequency values are now combined rather than being separate as they were in the multiplicative form,

$$y = \cos(\omega_c t+\phi_c)\cos(\omega_p t+\phi_p) = \frac{1}{2}[\cos((\omega_c-\omega_p)t+\phi_c-\phi_p)+\cos((\omega_c+\omega_p)t+\phi_c+\phi_p)] \tag{4.2}$$

4.2 Putting the Signal in the Parametric Form

The next step toward creating the least–squares algorithm is to put the system in a parametric model, which involves moving the desired values for estimation outside of the sinusoid. This is done by using the well known relationship between even multiple derivatives for sinusoids,

$$y^{(2)} = \frac{1}{2}[-(\omega_c-\omega_p)^2\cos((\omega_c-\omega_p)t+\phi_c-\phi_p)-(\omega_c+\omega_p)^2\cos((\omega_c+\omega_p)t+\phi_c+\phi_p)] \tag{4.3}$$

$$y^{(4)} = \frac{1}{2}[(\omega_c-\omega_p)^4\cdot\cos((\omega_c-\omega_p)t+\phi_c-\phi_p)+(\omega_c+\omega_p)^4\cdot\cos((\omega_c+\omega_p)t+\phi_c+\phi_p)]. \tag{4.4}$$

Through observing that the cosines are the same in both the derivatives, $y^{(4)}$ is written in terms of the lower even derivatives (4.3) and (4.2),

$$y^{(4)} + [(\omega_c-\omega_p)^2+(\omega_c+\omega_p)^2]y^{(2)} + [(\omega_c-\omega_p)^2\cdot(\omega_c+\omega_p)^2]y = 0.$$

To simplify notation and put the equation in a more recognizable form, let $\theta_1 = (\omega_c-\omega_p)^2+(\omega_c+\omega_p)^2$ and $\theta_2 = (\omega_c-\omega_p)^2\cdot(\omega_c+\omega_p)^2$.

The input signal y is the known value in the equation and θ_1 and θ_2 are the parameters to be estimated. Rearranging the equation with the known input on the left hand side and the unknown parameters on the right hand side,

$$y^{(4)} = -\theta_1 y^{(2)} - \theta_2 y.$$

The equation is transformed into the s-domain and a fourth order filter is inserted

to remove the need to know the derivatives of y.

$$\frac{s^4}{(s+\lambda)^4}[y] = -\theta_1 \cdot \frac{s^2}{(s+\lambda)^4}[y] - \theta_2 \cdot \frac{1}{(s+\lambda)^4}[y]$$
$$y - \frac{4\lambda s^3 + 6\lambda^2 s^2 + 4\lambda^3 s + \lambda^4}{(s+\lambda)^4}[y] = -\theta_1 \frac{s^2}{(s+\lambda)^4}[y] - \theta_2 \frac{1}{(s+\lambda)^4}[y]. \quad (4.5)$$

Now the equation is in a recognizable form, similar to that of equation (3.6) if the right hand side were put in vector form. Defining

$$\theta = \begin{pmatrix} \theta_1 \\ \theta_2 \end{pmatrix},$$
$$\Phi = \begin{pmatrix} \frac{-s^2}{(s+\lambda)^4}[y] \\ \frac{-1}{(s+\lambda)^4}[y] \end{pmatrix},$$
$$Y = y - \frac{4\lambda s^3 + 6\lambda^2 s^2 + 4\lambda^3 s + \lambda^4}{(s+\lambda)^4}[y],$$

the equation is now in the parametric form of equation (3.1).

Now the vectors are simply placed into the appropriate places in the least–squares adaptive filter, as derived in (3.12),

$$\begin{pmatrix} \dot{\hat{\theta}}_1 \\ \dot{\hat{\theta}}_2 \end{pmatrix} = \Gamma \begin{pmatrix} \frac{-s^2}{(s+\lambda)^4}[y] \\ \frac{-1}{(s+\lambda)^4}[y] \end{pmatrix} \times$$
$$\left\{ y - \frac{4\lambda s^3 + 6\lambda^2 s^2 + 4\lambda^3 s + \lambda^4}{(s+\lambda)^4}[y] + \hat{\theta}_1 \frac{s^2}{(s+\lambda)^4}[y] + \hat{\theta}_2 \frac{1}{(s+\lambda)^4}[y] \right\} \quad (4.6)$$

The update equation for Γ from equation (3.11) with the given Φ vector becomes

$$\dot{\Gamma} = \beta\Gamma - \Gamma \begin{pmatrix} \frac{-s^2}{(s+\lambda)^4}[y] \\ \frac{-1}{(s+\lambda)^4}[y] \end{pmatrix} \begin{pmatrix} \frac{-s^2}{(s+\lambda)^4}[y] & \frac{-1}{(s+\lambda)^4}[y] \end{pmatrix} \Gamma. \quad (4.7)$$

Setting $\beta > 0$, the forgetting factor component is included to increase the speed of convergence. The ability for Γ to adjust and update allows $\hat{\omega}_c$ and $\hat{\omega}_p$ to change by orders of magnitude since the covariance can compensate quickly and bring the system to steady state.

Therefore the *continuous-time recursive least–squares algorithm with forgetting factor* using equations (4.6) and (4.7) is created to estimate θ_1 and θ_2. However θ is a combination of the desired frequency values, thus the frequencies are extrapolated from $\hat{\theta}$

$$\hat{\omega}_c = \frac{\sqrt{\hat{\theta}_1 + 2\sqrt{\hat{\theta}_2}}}{2}$$

$$\hat{\omega}_p = \frac{\sqrt{\hat{\theta}_1 - 2\sqrt{\hat{\theta}_2}}}{2}$$

4.3 Proof of Conditions for Φ

In order for the algorithm to be stable and converge to the correct values, Φ must satisfy PE and $\Phi \in \mathcal{L}_\infty$.

Since the input y is given, the complete Laplace form of Φ becomes

$$\Phi = \begin{pmatrix} \frac{-s^3(s^2+\omega_c^2+\omega_p^2)}{(s+\lambda)^4(s^2+(\omega_c+\omega_p)^2)(s^2+(\omega_c-\omega_p)^2)} \\ \frac{-s(s^2+\omega_c^2+\omega_p^2)}{(s+\lambda)^4(s^2+(\omega_c+\omega_p)^2)(s^2+(\omega_c-\omega_p)^2)} \end{pmatrix}. \tag{4.8}$$

The definition of PE given in equation (3.13) is in the time domain, so (4.8) must first be transformed into the time domain. Taking the inverse Laplace transformation, Φ is rewritten in the time domain as

$$\Phi = \begin{pmatrix} \frac{\alpha\sin((\omega_c+\omega_p)t)+\beta\sin((\omega_c-\omega_p)t)+\kappa\cos((\omega_c+\omega_p)t)+\rho\cos((\omega_c-\omega_p)t)+(at^3+bt^2+ct+d)e^{-\lambda t}}{(\lambda^2+(\omega_c+\omega_p)^2)^4\cdot(\lambda^2+(\omega_c-\omega_p)^2)^4} \\ \frac{\sigma\sin((\omega_c+\omega_p)t)+\mu\sin((\omega_c-\omega_p)t)+\eta\cos((\omega_c+\omega_p)t)+\nu\cos((\omega_c-\omega_p)t)+(ft^3+gt^2+ht+k)e^{-\lambda t}}{(\lambda^2+(\omega_c+\omega_p)^2)^4\cdot(\lambda^2+(\omega_c-\omega_p)^2)^4} \end{pmatrix}, \tag{4.9}$$

where $\alpha, \beta, \kappa, \rho, \sigma, \mu, \eta, \nu, a, b, c, d, f, g, h, k$ are real constants dependent on ω_c, ω_p, and λ. Now Φ is multiplied by its transpose to create a four by four matrix,

$$\Phi\Phi^T = \begin{pmatrix} \phi_1^2 & \phi_1\phi_2 \\ \phi_2\phi_1 & \phi_2^2 \end{pmatrix}.$$

Since the actual calculation of the matrix is rather complex, some observations will be made by examining the vector given in equation (4.9). In the matrix, the diagonal terms are the squared values of ϕ_1 and ϕ_2. Hence the diagonals are a summation of squared sines and cosines, multiplicative sines and cosines, and exponential functions. Setting $T_0 = \pi$ in the integral of equation (3.13), Φ is PE if the integral of $\Phi\Phi^T$ is bounded and always greater than or equal to zero. Using the integral identities for sine and cosine[1] the sinusoidal squared and product terms are evaluated. The constants in front of all the sine and cosine products are positive and the

[1]The integral identities used in the calculation are:

$$\frac{1}{\pi}\int_t^{t+\pi} \sin(A\tau)\sin(B\tau)\,\mathrm{d}\tau = \frac{\sin((A-B)(t+\pi))}{2(A-B)\pi} - \frac{\sin((A+B)(t+\pi))}{2(A+B)\pi}, \\ + \frac{\sin((A+B)t)}{2(A+B)\pi} - \frac{\sin((A-B)t)}{2(A-B)\pi}$$

$$\frac{1}{\pi}\int_t^{t+\pi} \cos(A\tau)\cos(B\tau)\,\mathrm{d}\tau = \frac{\sin((A-B)(t+\pi))}{2(A-B)\pi} + \frac{\sin((A+B)(t+\pi))}{2(A+B)\pi},$$

summation of the sine and cosine products results in a positive net value. The rest of the terms are multiplied by the exponential, $e^{-\lambda t}$ and since λ is a very large value, the exponential decays rapidly and can be ignored in calculating the value of the diagonals. Therefore, the values of ϕ_1^2 and ϕ_2^2 oscillate and are uniformly positive for all time intervals $[t, t+T_0]$. Figures 4.1 and 4.2 provide a graphical verification that the diagonal terms are bounded. The effect of the exponential decaying term is seen as the oscillations decrease and integrals settle to constant values. Since the integral is taken at each time step, the upper bound of the integral changes so that $T_0 = t_n$, where t_n is the last time value, while the lower bound remains constant at $t = 0$. Thus the condition of persistence of excitation for the given Φ is proved analytically and graphically confirmed through simulation.

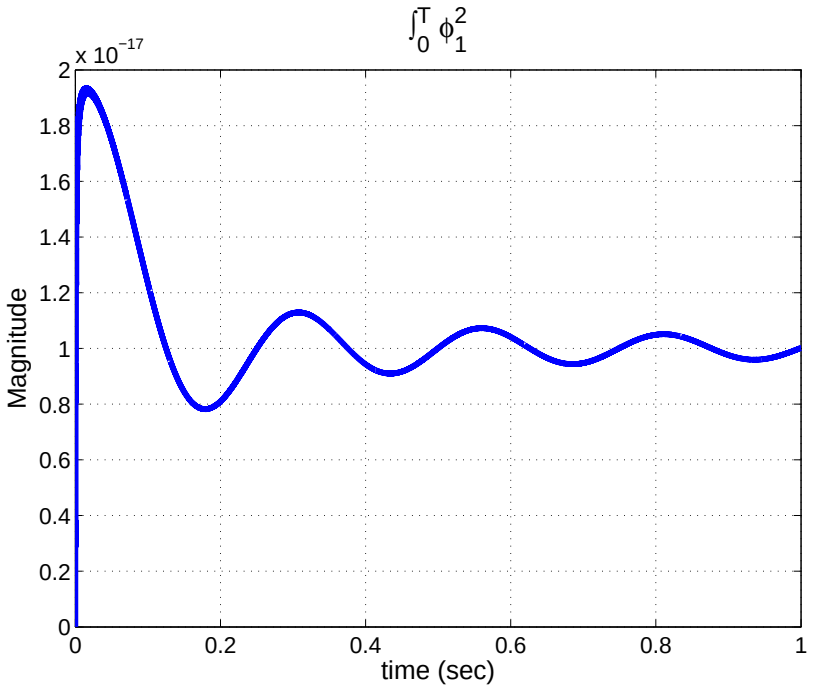

Figure 4.1: Integral of ϕ_1^2 to Confirm PE Condition

$$
\begin{aligned}
&- \frac{\sin((A+B)t)}{2(A+B)\pi} - \frac{\sin((A-B)t)}{2(A-B)\pi} \\
\frac{1}{\pi}\int_t^{t+\pi} \sin(A\tau)\cos(A\tau)\,\mathrm{d}\tau &= -\frac{\cos^2(A(\pi+t)))}{2\pi A} + \frac{\cos^2(At)}{2\pi A} \\
\frac{1}{\pi}\int_t^{t+\pi} \sin(B\tau)\cos(A\tau)\,\mathrm{d}\tau &= \frac{\cos((A-B)(\pi+t))}{2\pi(A-B)} - \frac{\cos((A+B)(\pi+t)))}{2\pi(A+B)} \\
&+ \frac{\cos((A+B)t)}{2\pi(A+B)} - \frac{\cos((A-B)t)}{2\pi(A-B)}
\end{aligned}
$$

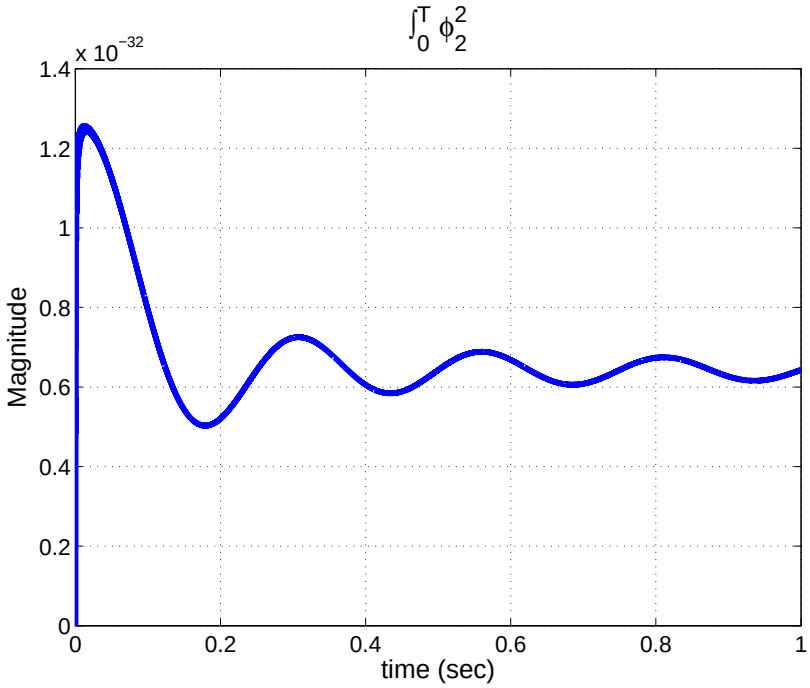

Figure 4.2: Integral of ϕ_2^2 to Confirm PE Condition

Starting from equation (4.9) the maximum absolute value needs to be less than infinity. Since Φ consists of exponential decaying terms and sinusoids, the maximum value is bounded. Thus, $\Phi < \infty, \forall t$ and the condition of L-infinity is satisfied.

Since both conditions on Φ have been verified to hold true, the adaptive filter given in equations (4.6) and (4.7) is ensured to be stable and converge to the correct values.

4.4 Simulation of Estimating the Frequencies

The values of λ, β, and Γ_0 should be chosen based on the order of magnitude of the carrier frequency. Since λ acts as a filter, it should be of the same order of magnitude and as close in value to ω_c as possible. β is the main value that affects the rate of convergence and can be larger for higher frequency values than lower frequencies since higher frequency signals means faster oscillations. If β is too large then not enough data is taken into account. The value of Γ_0 is the initial error between the estimated parameter values and the actual values. Since the initial value of the estimate $\hat{\theta}$ is zero, the error is very large and the greater the order of magnitude of ω_c, the greater Γ_0. The following simulation illustrates the

identification of two frequencies, $\omega_c = 2\pi \cdot 100 \times 10^3$ rad/sec and $\omega_p = 2\pi 2$ rad/sec. Using $\lambda = 2\pi \cdot 100 \times 10^3$, and $\beta = 10500$, figure 4.3 shows the estimate of ω_c and figure 4.4 shows the estimate of ω_p.

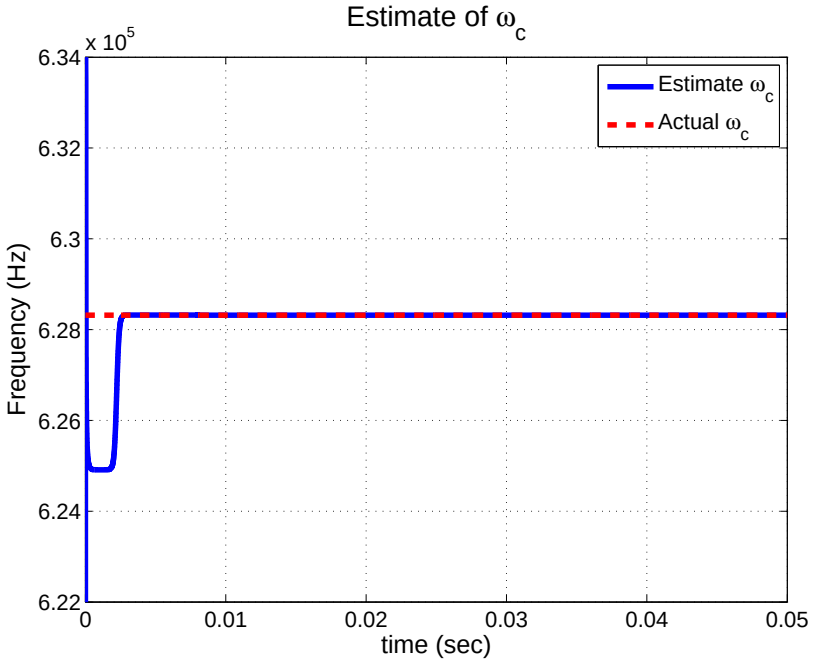

Figure 4.3: Plot of $\hat{\omega}_c$ for $\omega_c = 2\pi 100e3 \approx 6.2832e5$ rad/sec

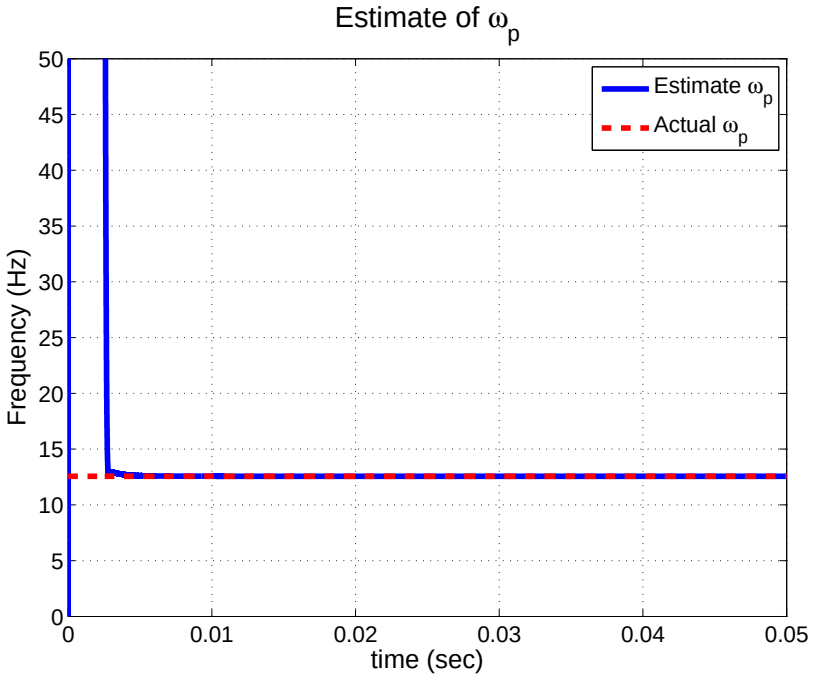

Figure 4.4: Plot of $\hat{\omega}_p$ for $\omega_p = 2\pi 2 \approx 12.566$ rad/sec

4.5 Simulations with Noise

In the previous section, the frequencies were estimated with no noise input. Now the effect of additive white noise on the incoming signal is analyzed, $y = \cos((\omega_c + \omega_p)t + \phi_c + \phi_p) + \cos((\omega_c - \omega_p)t + \phi_c - \phi_p) + n$, where n is noise. The noise will have the greatest affect on the signal at the zero crossings, when the amplitude of the signal is small and the signal to noise ratio is large. Since the gradient method is used to minimize the cost function, the max/min values of the signal are also an area of concern since the gradient goes to zero at these points. The noise has such a large effect on the parameter estimates due to the large forgetting factor, which focuses only on the most recent data. This results in large estimation errors in the minimal gradient regions since the noise corrupts the data. Thus it is important in these regions to have a small forgetting factor so that the data further from the zero crossings and zero gradient areas are incorporated into the cost. Smaller frequencies are more affected by noise since the signal remains near the zero crossing and max/min values for a longer period of time. Figures 4.5 and 4.6 visually demonstrate how the noise effect is proportional to the frequency and causes greater divergence in lower frequency signals when the forgetting factor is too large. The simulations use actual white noise data from the track with a variation between $\pm 2 \times 10^{-3}$, $\omega_c = 2\pi \cdot 1 \times 10^3$, $\lambda = 2\pi \cdot 1 \times 10^3$, and $\beta = 2050$. Two different low frequency values were used; first the frequency was set to $\omega_p = 2\pi \cdot 1 \times 10^2$ and then the frequency was lowered to $\omega_p = 2\pi 2$.

By reducing the forgetting factor, the effects of the noise can be reduced; however, the convergence of the estimate becomes too slow for practical implementation of a small constant forgetting factor. In order to allow for both quick convergence initially and incorporate a larger set of data points once the estimate has converged, the forgetting factor must adjust online. Since the forgetting factor should not decrease until the system has reached convergence, the value of the forgetting factor should be proportional to the change in frequency between each time step. By taking the absolute value of the derivative of the frequency estimate, the forgetting factor can be tuned to allow for quick convergence and minimal noise effect at the zero crossings and zero gradient regions. Figure 4.7 shows the improvement in estimation using a varying forgetting factor and figure 4.8 shows the values of β.

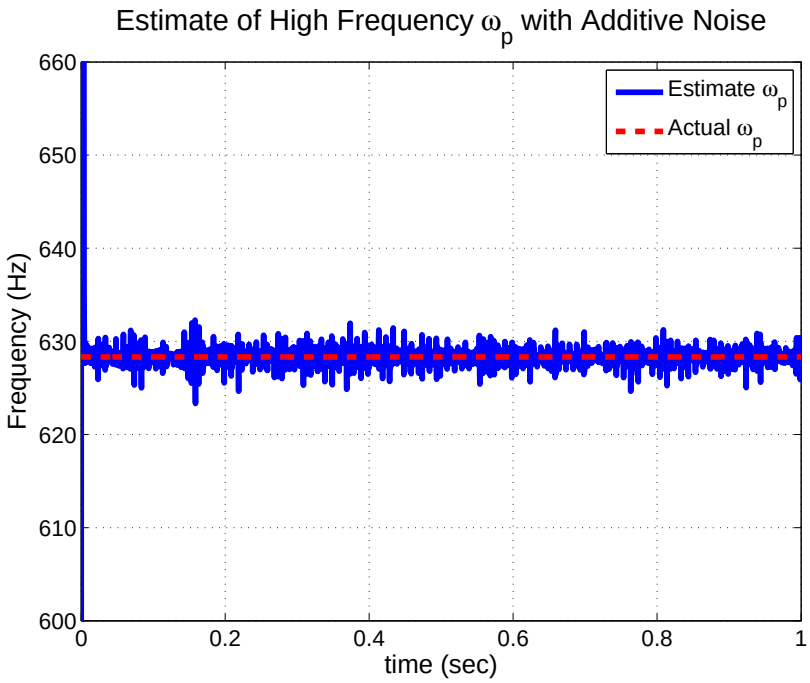

Figure 4.5: Estimate of $\omega_p = 2\pi \cdot 1 \times 10^2 \approx 628.32$ with Additive Noise

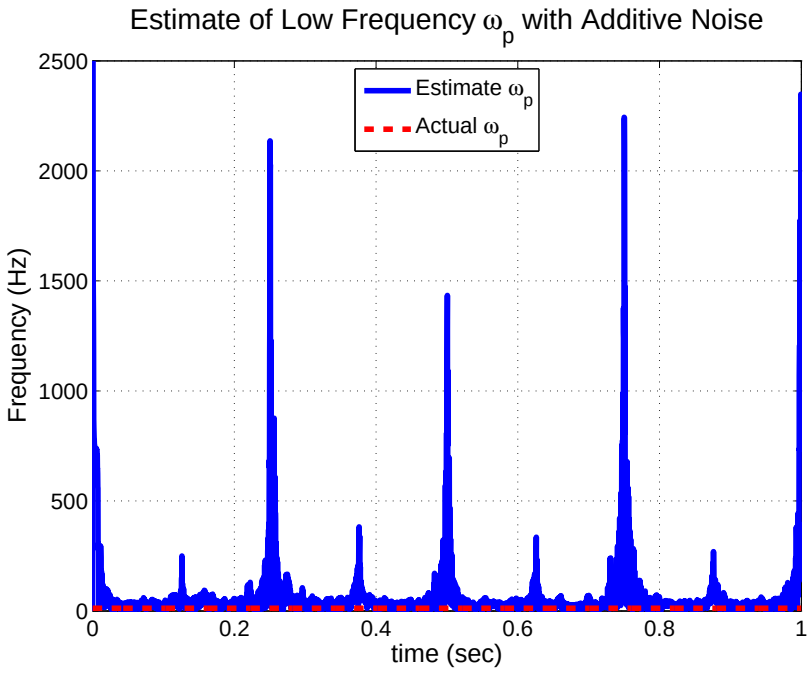

Figure 4.6: Estimate of $\omega_p = 2\pi 2 \approx 12.566$ with Additive Noise

4.6 Varying Frequency

The previous sections dealt with constant frequencies and additive noise. Due to the train moving, the low frequency signal will not always be constant but can

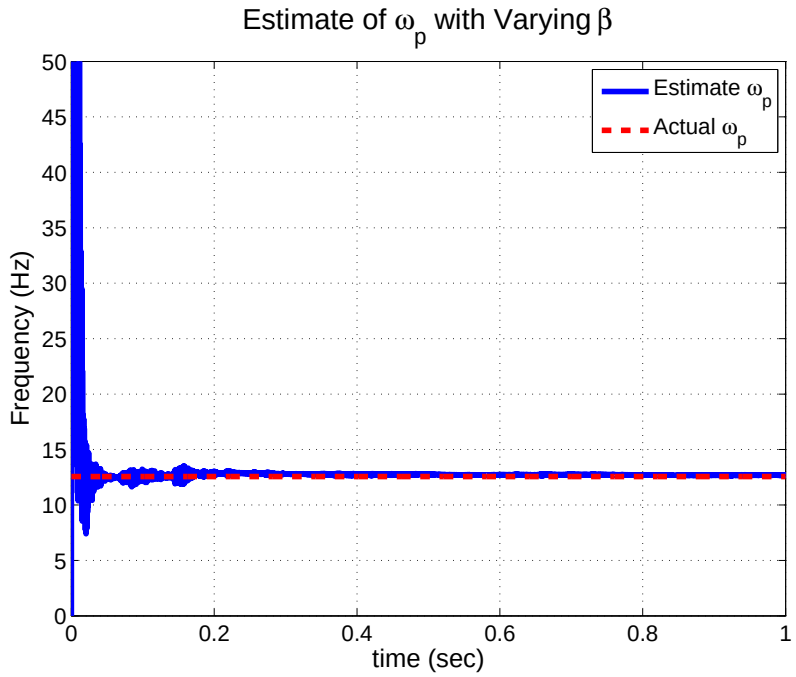

Figure 4.7: Estimate of $\omega_p = 2\pi 2 \approx 12.566$ with Additive Noise and Varying Forgetting Factor

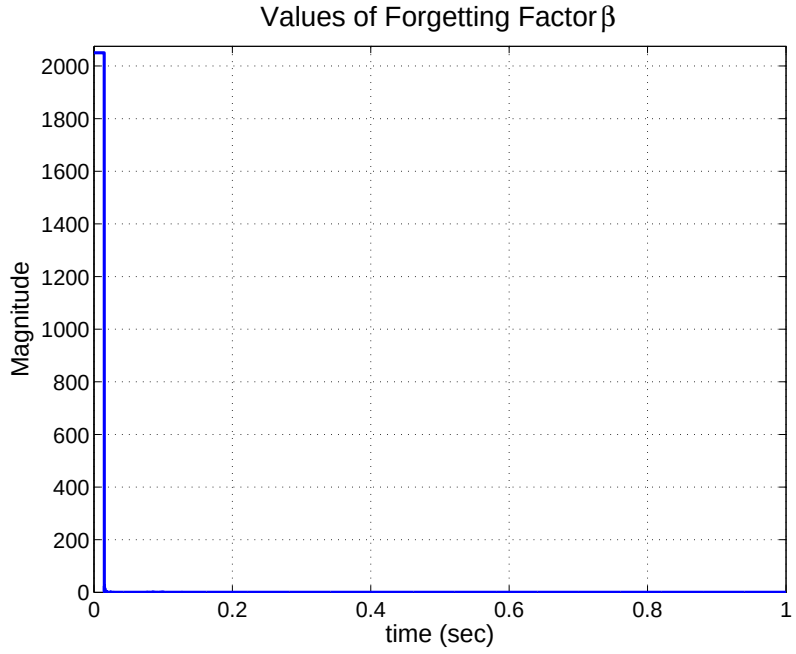

Figure 4.8: Values of Forgetting Factor β, Based on Slope of $\hat{\omega}_p$

vary from $0 - 40$Hz. The maximum acceleration of the train is 4m/s^2, meaning that the maximum change in velocity is $\Delta v = 4\Delta t$. When the low frequency signal changes, the estimate of the high frequency signal should remain unaffected. The

low frequency signal is a function of the velocity of the train according to $\omega_c = 2\pi\frac{v}{\lambda}t$, where $\lambda \approx 0.452$m is the wavelength of the LSM coils. Therefore, the maximum change in frequency becomes $\Delta\omega_p = 2\pi\frac{4}{0.452}\Delta t$. The following simulations keep ω_c constant at $2\pi \cdot 1 \times 10^3$ while ω_p increases with a constant slope from $2\pi \cdot 2$ to $2\pi \cdot 4$ at a rate $\Delta\omega_p = 25\Delta t$. Figure 4.9 shows the estimate of the high frequency remaining unaffected by the changing lower frequency. Figure 4.10 shows the estimate of the low frequency tracking the ramp change and converging once the frequency settles to a constant. The estimate takes longer to converge once the frequency stops changing due to the forgetting factor being small, whereas initially the forgetting factor is much greater. The convergence of the frequency estimate can be increased by putting a lower bound on the forgetting factor. However, the bound cannot be too high otherwise the spikes due to noise at the zero gradient of the signal will return. Figure 4.11 shows the estimate of ω_p when there is a lower bound of 20 on the forgetting factor. The convergence of the estimate once the frequency has settled is must faster than when there is no limit on the forgetting factor. However, during the ramping portion, the estimate diverges much further away from the actual value. This is due to the modulated signal appearing to oscillate faster than it actually is since the low frequency signal is varying. This compression of the signal is seen in figure 4.12.

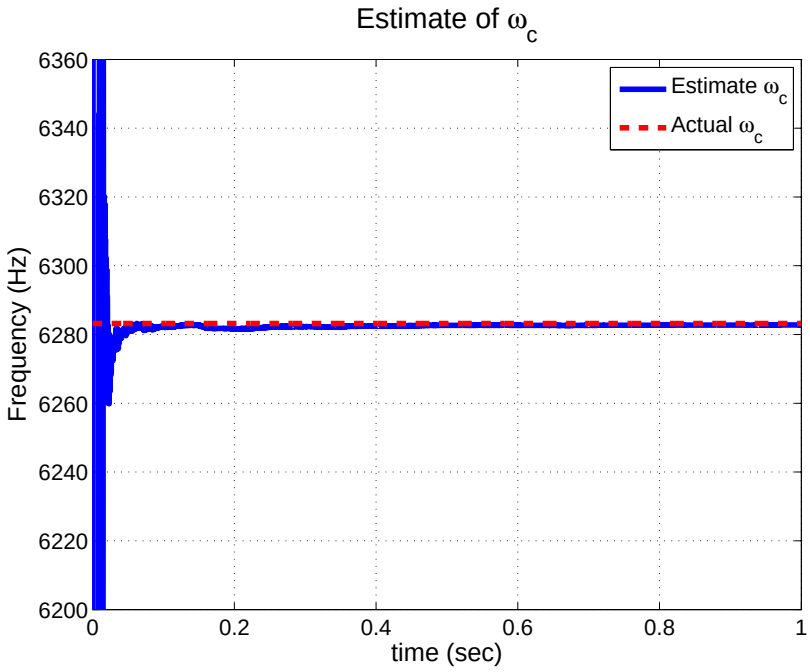

Figure 4.9: Estimate of ω_c While ω_p is Varying

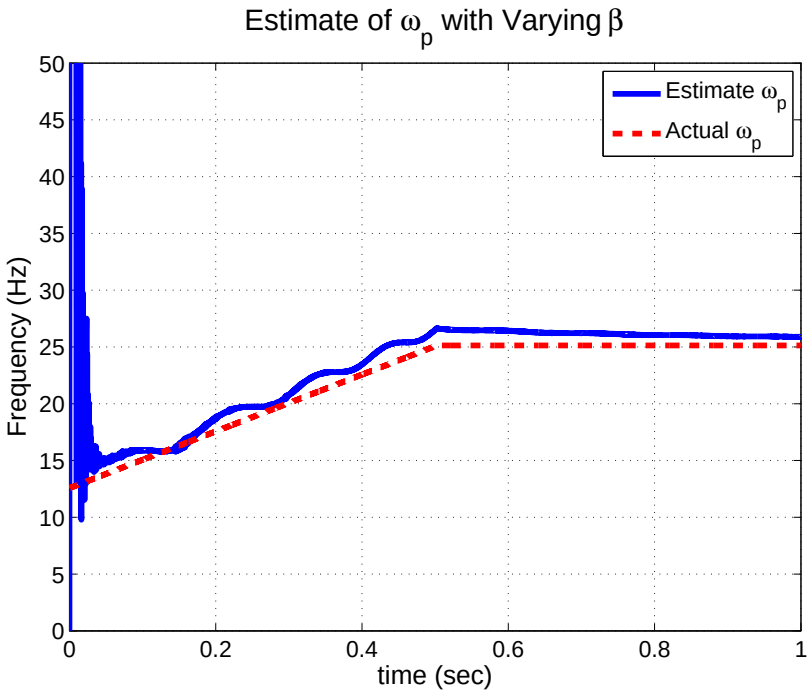

Figure 4.10: Estimate of Varying ω_p, No Lower Bound on β

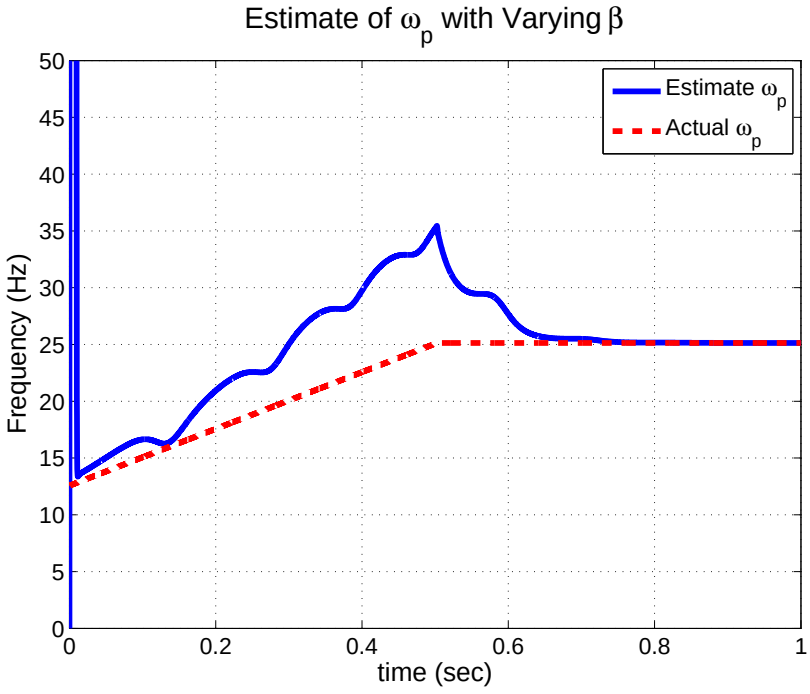

Figure 4.11: Estimate of Varying ω_p, Lower Bound of 20 on β

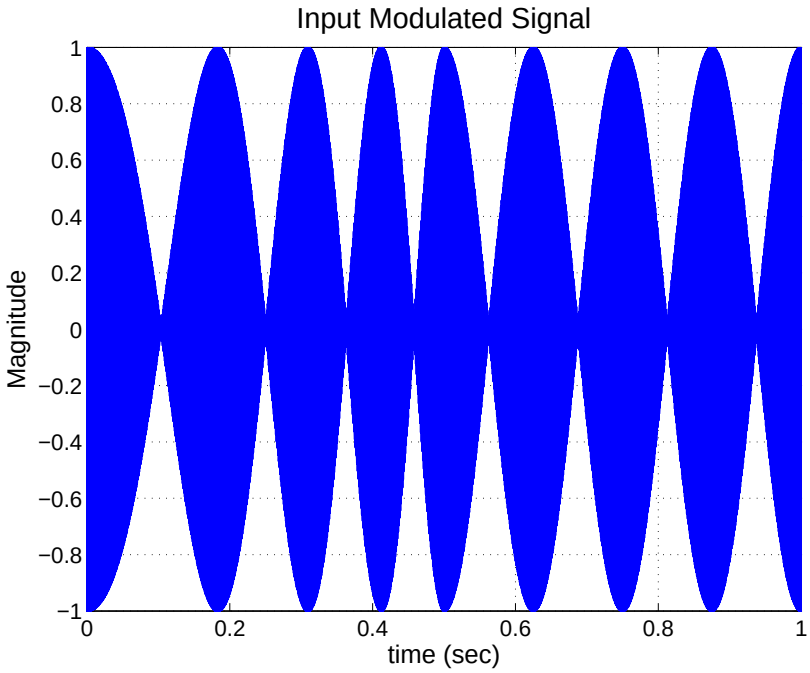

Figure 4.12: Modulated Signal of Time Varying Frequency

5

Extremum Seeking for Phase Estimation

In the previous chapter, only the frequency of the sinusoids were estimated since the phases are not time dependent. An additional algorithm, extremum seeking, will now be introduced to estimate the phase of the high frequency signal. Unlike the least–squares algorithm, extremum seeking only estimates one of the phases and due to the large difference in frequency between the two sinusoids, it is not realistic to estimate both phases using the same extremum seeking loop. In order to estimate the phase, the maximum or minimum of a nonlinear function is utilized to minimize the error between the actual value and the estimate. This chapter will first introduce a nonlinear mapping to minimize the error at the local maximum of cosine at zero degrees. A proof of convergence and stability for the extremum seeking loop will be shown to ensure the phase estimate reaches the actual value, given the output of the nonlinear map. Simulation results will be shown to confirm the analysis.

5.1 Signal Map

From the given input signal, $\cos(\omega_c t + \phi_c)\cos(\omega_p t + \phi_p)$, the goal is to estimate the phase of the carrier sinusoid, ϕ_c. In order to minimize the error between the phase estimate and the actual value, the nonlinear mapping needs creates a cosine which is only a function of this error. First, the input signal is multiplied with an estimate of the carrier signal

$$\cos(\hat{\omega}_c t + \hat{\phi}_c) \cdot \cos(\omega_c t + \phi_c) \cdot \cos(\omega_p t + \phi_p). \tag{5.1}$$

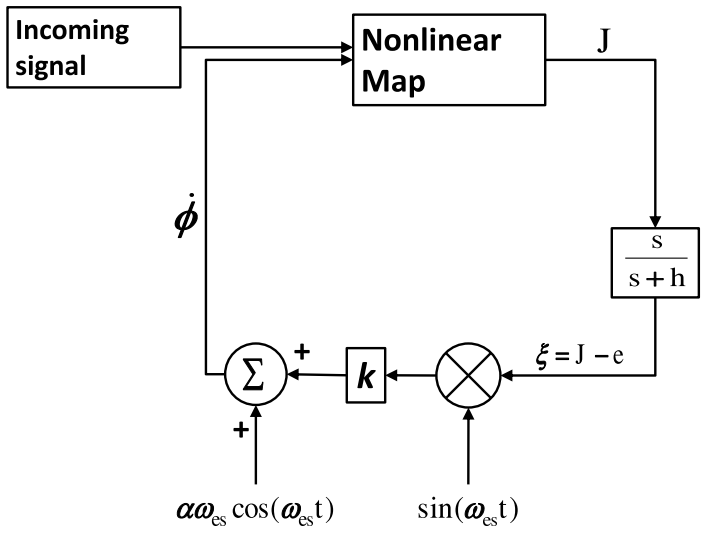

Figure 5.1: Block Diagram of Extremum Seeking Loop

The trig identity puts the cosines in an additive form,

$$\cos(\hat{\omega}_c t + \hat{\phi})\cos(\omega_c t + \phi)\cos(\omega_p t + \phi_p) = \frac{1}{2}\cos(\omega_p t + \phi_p)\Big\{\cos\Big((\hat{\omega}_c + \omega_c)t + \hat{\phi}_c + \phi_c\Big) + \cos\Big((\hat{\omega}_c - \omega_c)t + \hat{\phi}_c - \phi_c\Big)\Big\}.$$

A low pass filter at ω_c is applied to remove the double frequency and the absolute value of the remaining signals is taken so that the value of the cosines is always positive. Using the estimated frequency value of the carrier from the least–squares algorithm, the cosine becomes only a function of the phase error, with a multiplicative term from the position sinusoid. Assuming $\hat{\omega}_c \approx \omega_c$, the nonlinear map becomes

$$\frac{1}{2}\Big|\cos(\omega_p t + \phi_p)\cos\Big((\hat{\omega}_c - \omega_c)t + \hat{\phi}_c - \phi_c\Big)\Big| \approx \frac{1}{2}|\cos(\omega_p t + \phi_p)\cos(\hat{\phi}_c - \phi_c)|. \quad (5.2)$$

5.2 Extremum Seeking Loop

Figure 5.1 shows the block diagram for the extremum seeking loop. Equation (5.2) is the output of the nonlinear map into the extremum seeking loop,

$$J = q|\cos(\omega_p t + \phi_p)\cos(\phi - \phi^*)|, \quad (5.3)$$

with ϕ^* being the actual phase and ϕ being the input into the map as the estimate from the extremum seeking loop. Comparing (5.3) with (5.2), $q = 1/2$; however, a gain could be applied to change the value to any positive constant. Using the averaging method, the following analysis will prove the stability of the system, following a similar line of reasoning to that seen in [22] and [4]. Define $e = \frac{h}{s+h}[J]$ so that the output after the washout filter can be written as

$$\xi = \frac{s}{s+h}[J] = J - e. \tag{5.4}$$

Completing the rest of the extremum seeking loop, the differential equation for ϕ can be defined as

$$\dot{\phi} = \alpha\omega_{es}\cos(\omega_{es}t) + k\sin(\omega_{es}t)\xi. \tag{5.5}$$

Applying a change of coordinates

$$\tilde{\phi} = \phi - \phi^* - \alpha\sin(\omega_{es}t) \tag{5.6}$$

takes into account the sinusoidal excitation that enters the non-linear map. Replacing $\tau = \omega_{es}t$ to simplify the calculations, ξ is written in terms of the new coordinates

$$\xi = q\left|\cos\left(\frac{\omega_p}{\omega_{es}}\tau + \phi_p\right)cos(\tilde{\phi} + \alpha\sin(\tau))\right| - e. \tag{5.7}$$

$\tilde{\phi}$ should also be written as a differential equation, using equation (5.5),

$$\begin{aligned}\frac{d\tilde{\phi}}{d\tau} &= \frac{d\phi}{d\tau} - \frac{d\phi^*}{d\tau} - \frac{d}{d\tau}\alpha\sin(\tau)\\ &= \frac{1}{\omega_{es}}(\alpha\omega_{es}\cos(\tau) + k\sin(\tau)\xi) - \alpha\cos(\tau)\\ \frac{d\tilde{\phi}}{d\tau} &= \frac{1}{\omega_{es}}k\sin(\tau)\xi.\end{aligned} \tag{5.8}$$

Similarly, e can also be written as a differential equation

$$\frac{de}{d\tau} = \frac{h}{\omega_{es}}\xi. \tag{5.9}$$

Now the averaging method is applied to determine the equilibrium point. The system is periodic in intervals of 2π, making the average system the integral of equations (5.8) and (5.9) between 0 and 2π,

$$\begin{aligned}\frac{d\tilde{\phi}_{avg}}{d\tau} &= \frac{k}{\omega_{es}}\frac{1}{2\pi}\int_0^{2\pi}\sin(\tau)(q|\cos(\frac{\omega_p}{\omega_{es}}\tau + \phi_p)\cos(\tilde{\phi}_{avg} + \alpha\sin(\tau))| - e)\,\mathrm{d}\tau\\ &= \frac{k}{\omega_{es}}\frac{1}{2\pi}\left[q\int_0^{2\pi}\sin(\tau)\left|\cos\left(\frac{\omega_p}{\omega_{es}}\tau + \phi_p\right)\right|\cos(\phi_{avg})e^{j\alpha\sin(\tau)}\,\mathrm{d}\tau\right.\\ &\qquad\left. - \int_0^{2\pi}\sin(\tau)e_{avg}\,\mathrm{d}\tau\right],\end{aligned} \tag{5.10}$$

$$\frac{de_{avg}}{d\tau} = \frac{h}{\omega_{es}}\frac{1}{2\pi}\int_0^{2\pi}(q|\cos\left(\frac{\omega_p}{\omega_{es}}\tau+\phi_p\right)cos(\tilde{\phi}_{avg}+\alpha\sin(\tau))| - e_{avg})\,\mathrm{d}\tau$$
$$= \frac{h}{\omega_{es}}\frac{1}{2\pi}\left[q\int_0^{2\pi}\left|\cos\left(\frac{\omega_p}{\omega_{es}}\tau+\phi_p\right)\right|\cos(\phi_{avg})e^{j\alpha\sin(\tau)}\,\mathrm{d}\tau - \int_0^{2\pi}e_{avg}\,\mathrm{d}\tau\right]. \tag{5.11}$$

Since the integral of sine from 0 to 2π is zero, e in (5.10) is multiplied by zero and is eliminated from the average of ϕ. The integral in (5.10) and (5.11) is similar to that of a Bessel integral, except for the additional cosine term. Fortunately in this case $\omega_{es} \gg \omega_p$; consequently, $\omega_p/\omega_{es} \approx 0$ and $\cos(\frac{\omega_p}{\omega_{es}}\tau+\phi_p) \approx \cos(\phi_p) = C$, where C is a constant. This allows the integral to be written in the form of Bessel's first integral[1]. Using this simplification, the average systems become

$$\frac{d\tilde{\phi}_{avg}}{d\tau} = \frac{k}{\omega_{es}}qCJ_1(\alpha)\cos(\tilde{\phi}_{avg}), \tag{5.12}$$

$$\frac{de_{avg}}{d\tau} = \frac{h}{\omega_{es}}(qCJ_0(\alpha)\cos(\tilde{\phi}_{avg}) - e_{avg}). \tag{5.13}$$

Setting the left hand side to zero, the equilibrium points can be found at, $\tilde{\phi}_{avg} = \pm\pi/2$ and $e_{avg} = 0$. The Jacobian of (5.12) – (5.13) evaluated at $(\pi/2, 0)$ is

$$J_{avg} = -\frac{1}{\omega_{es}}\begin{bmatrix} kqCJ_1(\alpha) & 0 \\ hqCJ_0(\alpha) & h \end{bmatrix}. \tag{5.14}$$

Choosing $k, \alpha, h > 0$, since the equilibrium point is a maximum, $q > 0$, and since the absolute value is taken in the nonlinear map, $C \geq 0$, it can be concluded that J_{avg} is Hurwitz and the equilibrium for the average system is exponentially stable.

Note that the estimated phase, $\hat{\phi}$, also depends on ω_p since the cosine is coupled with the phase estimate. Since the phase estimate is also excited by the extremum seeking signal, $\cos(\omega_{es}t)$, the oscillation due to the extremum seeking is modulated with $\cos(\omega_p t)$. By adding a low pass filter to the output of the phase estimate and tuning the cutoff frequency, the variation at steady state can be reduced.

5.3 Simulation of Extremum Seeking

The following simulations illustrate the exponential convergence of $\hat{\phi}$ with various output filters to show how the effect of the modulation can be reduced. The high

[1]Bessel's first integral which can be derived from the Taylor series approximations, $J_1(a) = \frac{1}{2\pi}\int_0^{2\pi}e^{ja\sin(t)}\sin(t)dt$ and $J_0(a) = \frac{1}{2\pi}\int_0^{2\pi}e^{ja\sin(t)}dt$, is used in calculating the average system.

frequency signal and the estimated frequency were set to, $\hat{\omega}_c = \omega_c = 2\pi \cdot 1 \times 10^3$. The value of the extremum seeking frequency must be lower than the high frequency signal, although the faster the oscillations, the quicker the convergence, therefore $\omega_{es} = 2\pi \cdot 1 \times 10^2$. The low frequency signal is constant at $\omega_p = 2\pi \cdot 2$. The washout filter in the extremum seeking loop must be lower than the frequency of the extremum seeking sinusoid, so it is set to $\frac{s}{s+40}$. The phase offset of the carrier frequency, $\phi^* = \pi/4$. The low pass filter in the nonlinear map prior to entering the extremum seeking loop is $\frac{1\times10^3}{s+1\times10^3}$ and the initial guess for the phase estimate, $\hat{\phi}_0 = 0$. Figure 5.2 shows the exponential convergence of $\hat{\phi}$ to ϕ^* with the output filter of the phase estimate at $\frac{1\times10^3}{s+1\times10^3}$, allowing the correlation with ω_p. Figure 5.3 shows the convergence with the filter at $\frac{40}{s+40}$, removing some of the correlation with ω_p.

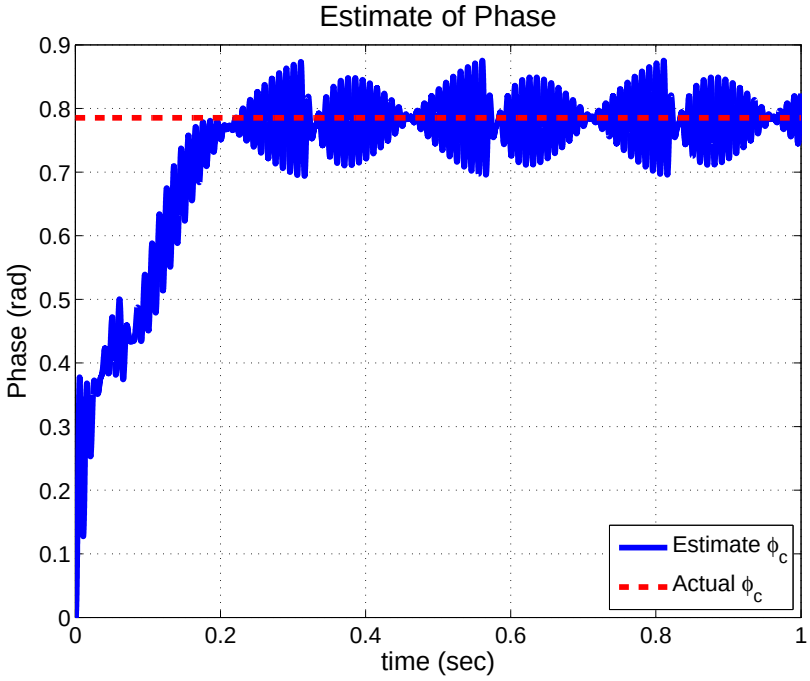

Figure 5.2: Estimate of Phase Using Extremum Seeking, $\phi = \pi/4$ with Output Filter $\frac{1\times10^3}{s+1\times10^3}$

The addition of noise to the incoming signal has little effect on the estimate of the phase. Since the local maximum is used to find the estimate, additional noise on the input data has less of an effect than other estimation algorithms. In addition, the filtering reduces the amount of noise that propagates through the loop. White noise from the track, with limits of $\pm 2 \times 10^{-3}$, was added to the incoming signal. Figure 5.4 shows that the noise has such a minimal effect on the estimate, that it

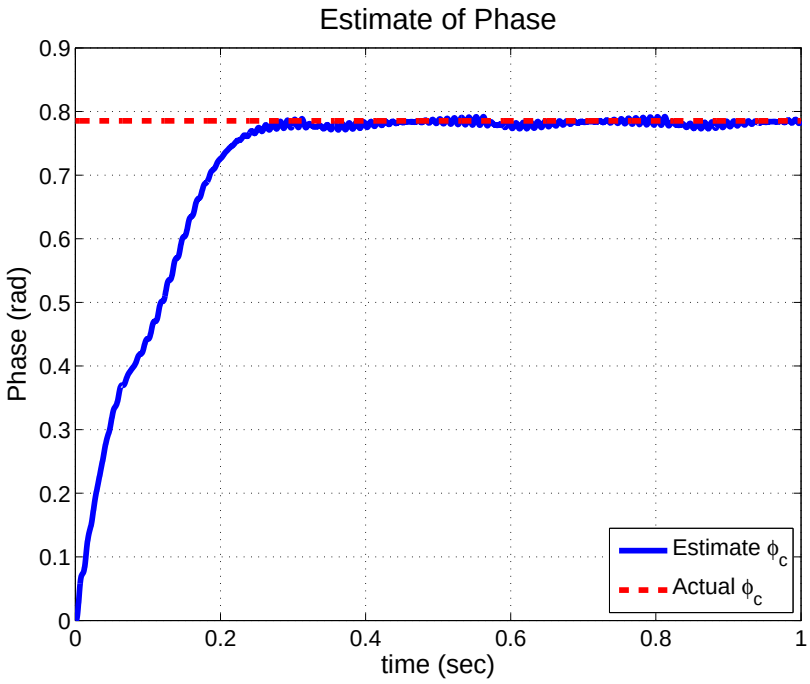

Figure 5.3: Estimate of Phase Using Extremum Seeking, $\phi = \pi/4$ with Output Filter $\frac{40}{s+40}$

is difficult to distinguish any difference from the estimate without noise. Since this level of noise did not really effect the estimate, a larger noise level of ± 2 is added to show the effects of noise. Figure 5.5 shows that the noise causes a slight divergence in the steady state value, but the system still appears stable.

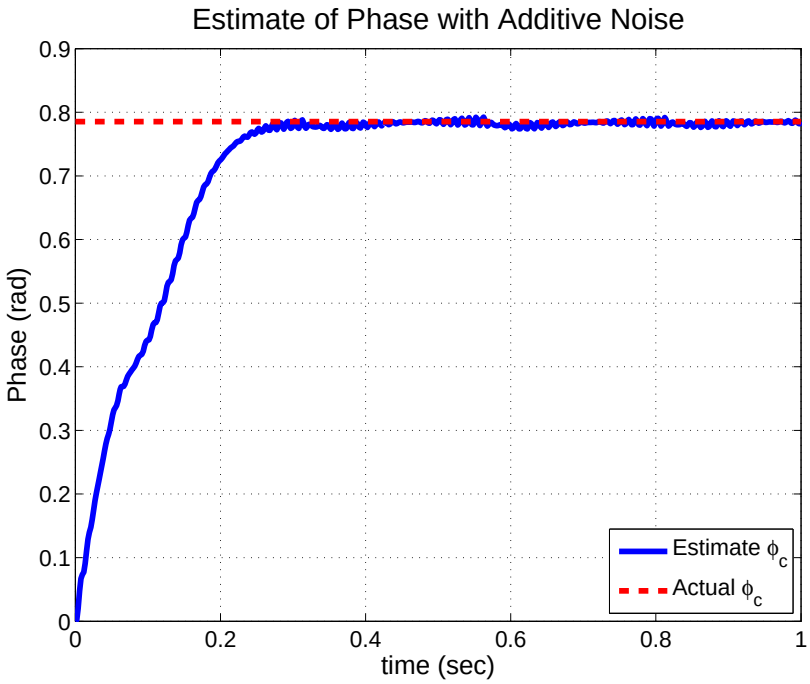

Figure 5.4: Estimate of Phase, $\phi_c = \pi/4$ with Additive Noise, $\pm 2 \times 10^{-3}$

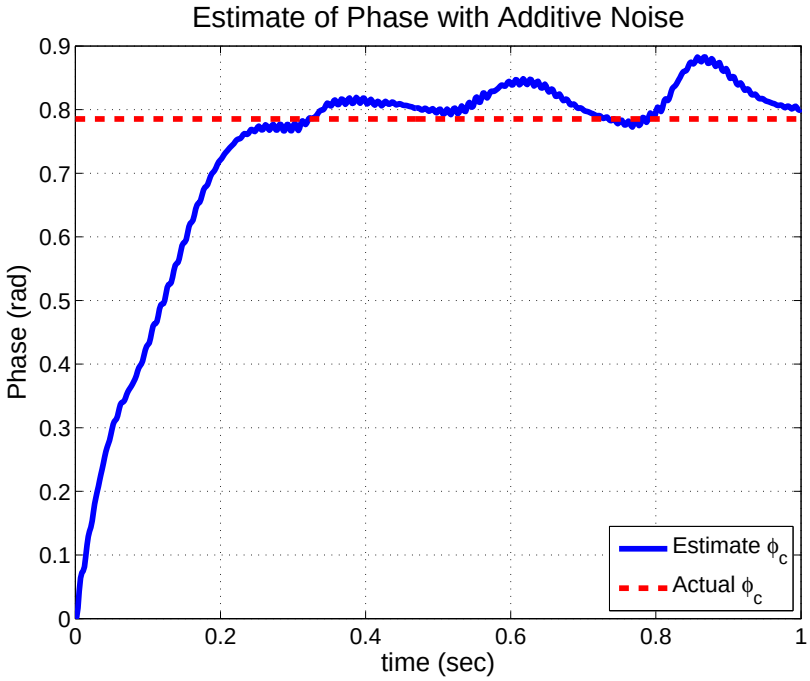

Figure 5.5: Estimate of Phase, $\phi_c = \pi/4$ with Additive Noise, ± 2

6

Combining Frequency and Phase Estimation

Now that both the frequency and phase have been determined, the two algorithms are used in conjunction to produce the actual desired output, $\cos(\omega_p t + \phi_p)$. The input of the modulated signal is sent to both the frequency and phase estimator. Since the frequency takes time to converge, the phase estimator needs some other source to use as the frequency input into the nonlinear mapping. The initial guess of the frequency is used until the estimated frequency converges. Once the estimated frequency has converged, the extremum seeking nonlinear map switches over and uses the estimate rather than the initial guess. The estimate of the frequency and phase for the high frequency signal are used to reconstruct the signal, $\cos(\hat{\omega}_c t + \hat{\phi}_c)$. This reconstructed estimate signal is multiplied by the modulated input, to demodulate the signal. When the frequency and phase estimates converge to the actual values, the high frequency signal is removed, leaving only the position signal from the coils. Figure 6.1 shows the demodulated signal corresponding to the low frequency sinusoid, with a slight phase offset from the low pass filter.

The demodulation should also be accurate when the train is accelerating and decelerating. When the train is stationary, the frequency of the coil's sinusoid is zero and the sinusoid remains at a constant value corresponding to the phase offset. The following simulation shows the frequency decreasing from $\omega_{p_i} = 2\pi$ to 0 at a rate of -4π. The frequency settles at 0 for half a second and then the frequency increases with a slope of 4π. The phase offset of the low frequency signal, $\phi_p = \frac{\pi}{4}$, causes the coil sinusoid to have a constant value of $\frac{1}{\sqrt{2}}$ when the frequency is zero.

As seen in figure 6.2, the demodulation is accurate except for a slight error when the slope transitions to and from zero, but it quickly recovers.

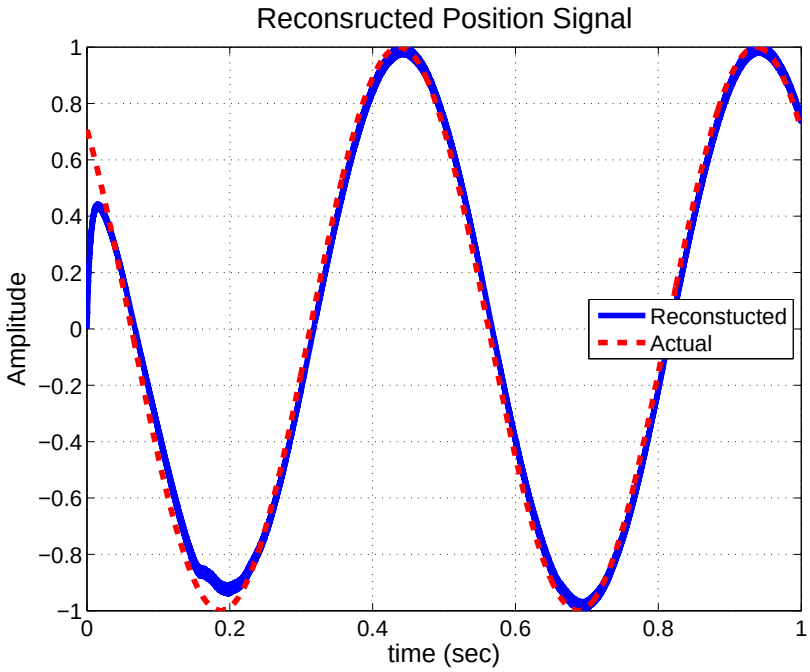

Figure 6.1: Demodulated Sinusoid of Coils

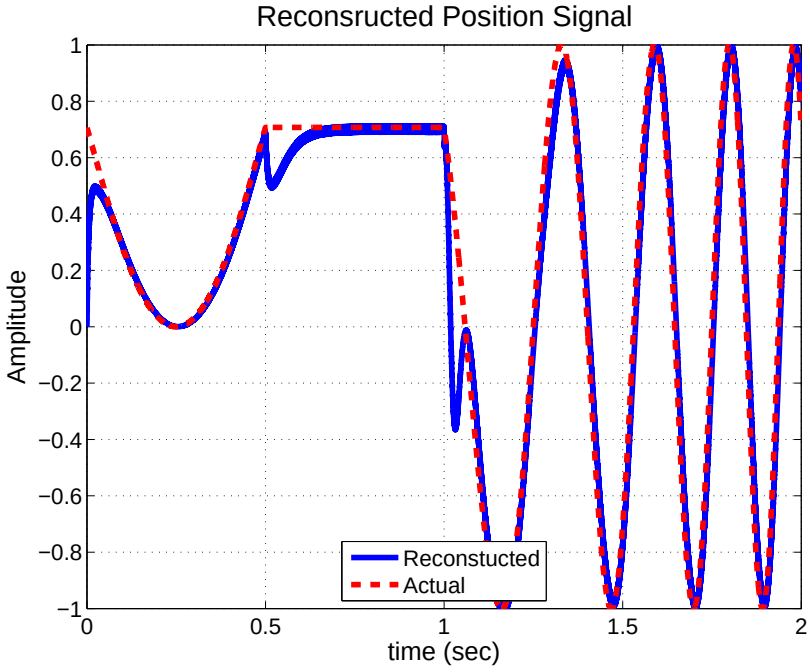

Figure 6.2: Demodulated Sinusoid of Coils with Varying Frequency

7

Conclusion

The objective of this thesis is to estimate the frequency and phase of modulated sinusoids. The frequency of both signals are estimated using the *continuous-time recursive least–squares algorithm with forgetting factor*. Extremum seeking uses the maximum located at zero degrees to estimate the phase of the high frequency signal. Both algorithms are stable and converge exponentially, even in the presence of noise.

After reviewing the basic operational components for maglev trains, Chapter 2 provided a more in-depth look at the specific area of propulsion and position tracking. The importance of knowing the train's position for LSM propulsion of the train was explained. The signal processing theory laid out how the high frequency signal from the drive coil on the train modulates with the sinusoids of the coils on the track. The mathematical derivation for estimating the position using the d-q frame was derived. Then the demodulation method used in this thesis was introduced.

The theory of the least–squares algorithm reviewed in Chapter 3 began with creating the parametric model of a system for use in the cost function. The inclusion of a forgetting factor focuses the cost function on the most recent data, increasing the convergence rate. By applying the zero gradient condition of the cost function, the equations for updating the parameter estimate and gain matrix are derived. A proof of convergence and stability is reviewed and shows that the parameters will converge exponentially. The pure least–squares algorithm, without the forgetting factor, was compared to the Kalman filter, showing the similarities between the two. However, without a forgetting factor, the algorithm takes too long to converge and hence, the least–squares with forgetting factor algorithm is superior in this application.

Chapter 4 used the least-squares algorithm to estimate the frequencies of the

modulated sinusoids. First the input signal was put in the parametric form. Using the unique characteristics of sinusoid derivatives, the parameters were placed in a multiplicative relationship with the input signal. The simulations showed the exponential convergence of the frequencies. By allowing the forgetting factor to vary, noise added to the signal removed the instability of the estimates in the zero gradient regions. Hence the algorithm is able to handle additive noise and still converge to the correct values.

Chapter 5 estimated the phase of the high frequency signal using extremum seeking. The non-linear map removes the high frequency component from the cosine so that the estimated phase converges to the actual value when the cosine is maximized at zero degrees. Completing the extremum seeking loop, the stability of the method was confirmed, even with the presence of the low frequency signal being modulated with the phase error. The use of extremum seeking for phase estimation, rather than phase locked loops or adaptive filtering, is a novel approach that allows the phase to be estimated, even in the presence of the modulated signal where the cosine of the lower frequency is correlated with the phase estimate. In addition, extremum seeking can handle large levels of additive noise, making it a robust method.

In Chapter 6 the frequency and phase algorithms are combined to reconstruct the carrier signal. With this reconstructed signal, the modulated input is low pass filtered to obtain the single low frequency sinusoid of the track coils. The ability to demodulate the signal accurately is confirmed through simulations, not only for the constant frequency case, but also when the coil frequency varies and is equal to zero.

7.1 Future Work

In the Least–Squares Algorithm with Forgetting Factor, the addition of noise was dealt with using a varying forgetting factor to handle the zero gradient regions. Since there will be three signals from the three phase coils on the track, rather than using a single data input, all three data inputs can be utilize to estimate the frequencies. Because all the signals are separated by a $\frac{2\pi}{3}$ phase shift, they will not have zero gradient instabilities at the same point; hence, ignoring the estimate which is inaccurate, the other two signals accurately estimate the frequencies, providing stability for the algorithm. This would provide an alternative method of handling

noise rather than varying the forgetting factor. A variation on the Kalman filter from chapter 3 or applying an extended Kalman filter are other techniques which could be examined and compared to the least–squares algorithm with forgetting factor. Through comparing the converges rates and robustness to the addition of noise the best method could be implemented.

For phase estimation, the objective of this research was to investigate the extremum seeking algorithm's ability to estimate the phase. Since phase locked loops (PLL) are the standard for identifying phases, a comparison between these two methods could be examined. Since extremum seeking displays robustness to small signal to noise ratio data, if PLL has less robust estimation, this shows the advantage of applying extremum seeking. The convergence rate and complexity of applying the method also could determine the best technique to apply for the specific application.

Appendix A

Block Diagrams

The simulations done for this thesis were created using simulink. The extremum seeking block diagram in figure A.1 is for additive noise with output filter of $\frac{s}{s+100}$. The block diagram in figure A.2 for the least-squares simulation contains the noise and variable β, using constant frequency values.

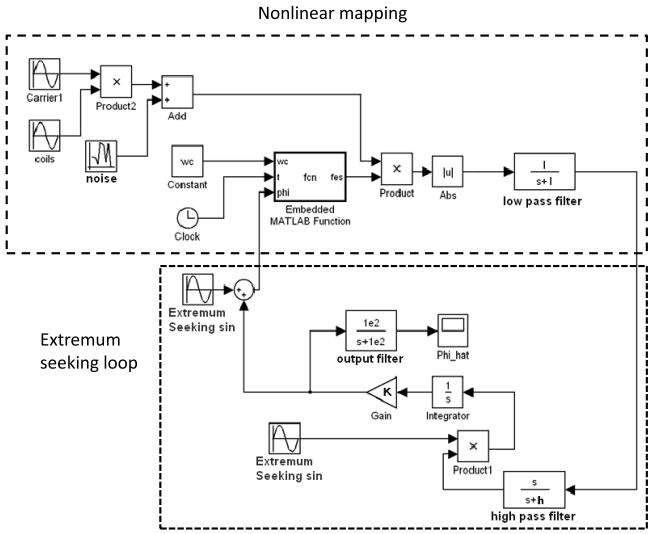

Figure A.1: Simulink Block Diagram of Extremum Seeking

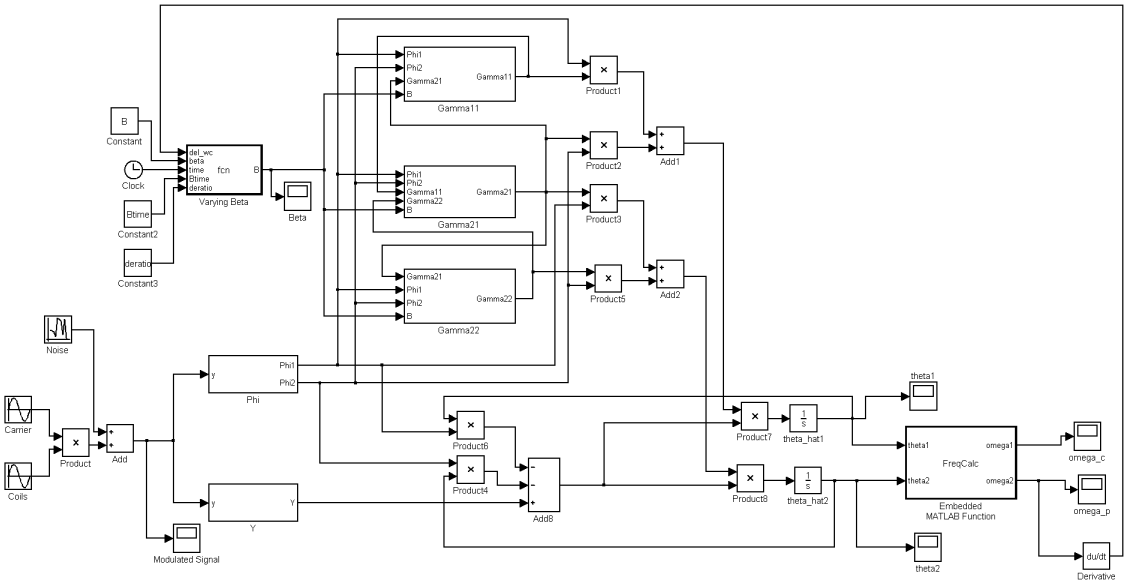

Figure A.2: Simulink Block Diagram of Least–Squares Algorithm with Vary β

Bibliography

[1] R. E. Best, *Phase-Locked Loops*. New York: McGraw-Hill, 2003.

[2] A. A. Bobtsov and D. A. Romasheva, "Frequency estimator of a biased sinusoid," in *46th IEEE Conference on Decision and Control*, 2007, pp. 5534–5538.

[3] B. Borowy, "Non-optical position sensor," 2008, internal document.

[4] J. Cochran and M. Krstic, "Source seeking with a nonholonomic unicycle without position measurements and with tuning of angular velocity part i: Stability analysis," in *46th IEEE Conference on Decision and Control*, 2007, pp. 6009–6016.

[5] F. Eastham and T. Cox, "Transient analysis of offset stator double sided short rotor linear induction motor accelerator," in *20th International Conference on Magnetically Levitated Systems and Linear Drives*, 2008, paper 5.

[6] J. F. Gieras and Z. J. Piech, *Linear Synchronous Motors: Transportation and Automation Systems*. Boca Ration, Florida: CRC Press, 2000.

[7] J. Gray, "Modeling and online parameter identification methods for electro-hydraulic valvetrain systems," Master's thesis, University of California, San Diego, 2009.

[8] M. Hou, "Amplitude and frequency estimator of a sinusoid," *IEEE Transactions on Automatic Control*, vol. 50, no. 6, pp. 855–858, 2005.

[9] L. Hsu, R. Ortega, and G. Damm, "A globally convergent frequency estimator," *IEEE Transactions on Automatic Control*, vol. 44, no. 4, pp. 698–713, 1999.

[10] P. A. Ioannou and J. Sun, *Robust Adaptive Control*. Upper Saddle River, New Jersey: Prentice-Hall, Inc., 1996.

[11] R. J. Kaye and E. Masada, "Comparison of linear synchronous and induction motors," Urban Maglev Technology Development Program Colorado Maglev Project, Tech. Rep., June 2004.

[12] R. Marino and P. Tomei, "Global estimation of n unknown frequencies," *IEEE Transactions on Automatic Control*, vol. 47, no. 8, pp. 1324–1328, 2002.

[13] V. Miambres, M. Milans, B. Vinagre, and E. Romero, "Comparison of controllers for a three-phase phase locked loop system under distorted conditions," in *Compatibility and power electronics 6th international conference–workshop*, 2009, pp. 79–85.

[14] R. D. Pascoe, "Command, control and communications - automatic train control system," in *20th International Conference on Magnetically Levitated Systems and Linear Drives*, 2008, paper 6.

[15] B. G. Quinn and E. J. Hannan, *The Estimation and Tracking of Frequency*. Cambridge, UK: Cambridge University Press, 2001.

[16] D. Rao and S.-Y. Kung, "Adaptive notch filtering for the retrieval of sinusoids in noise," *IEEE Transactions on Acoustics, speech, and signal processing*, vol. 32, no. 4, pp. 791–802, 1984.

[17] O. Rodriguez, "The new steel guideway," in *20th International Conference on Magnetically Levitated Systems and Linear Drives*, 2008, paper 1.

[18] B. F. L. Scala and R. R. Bitmead, "Design of an extended Kalman filter frequency tracker," *IEEE Transactions on Signal Processing*, vol. 44, no. 3, pp. 739–742, 1996.

[19] D. Simon, *Optimal State Estimation*. Hoboken, New Jersey: John Wiley and Sons, Inc., 2006.

[20] X. Xia, "Global frequency estimation using adaptive identifiers," *IEEE Transactions on Automatic Control*, vol. 47, no. 7, pp. 1188–1193, 2002.

[21] W. Xu, G. Sun, Y. Li, and L. Tan, "New equivalent circuits of single-sided linear induction motor," in *20th International Conference on Magnetically Levitated Systems and Linear Drives*, 2008, paper 4.

[22] C. Zhang, A. Siranosian, and M. Krstic, "Extremum seeking for moderately unstable systems and for autonomous vehicle target tracking without position measurements," *Automatica*, vol. 43, pp. 1832–1839, 2007.